PLGA-nanoparticles for intracellular delivery of the CRISPR-complex to elevate fetal globin expression in erythroid cells

Cruz, L.J.; Dijk, T. van; Vepris, O.; Li, T.M.W.Y.; Schomann, T.; Baldazzi, F.; ... ; Eich, C.

Biomaterials 268 (2021) 120580

Contents lists available at ScienceDirect

Biomaterials

journal homepage: www.elsevier.com/locate/biomaterials

PLGA-Nanoparticles for Intracellular Delivery of the CRISPR-Complex to Elevate Fetal Globin Expression in Erythroid Cells

Luis J. Cruz [a], Thamar van Dijk [b], Olena Vepris [a], Tracy M.W.Y. Li [a], Timo Schomann [a,c], Fabio Baldazzi [a], Ryo Kurita [d], Yukio Nakamura [e], Frank Grosveld [b], Sjaak Philipsen [b], Christina Eich [a,*]

[a] Translational Nanobiomaterials and Imaging, Department of Radiology, Leiden University Medical Center, the Netherlands
[b] Erasmus University Medical Center, Department of Cell Biology, Rotterdam, the Netherlands
[c] Percuros B.V, Leiden, the Netherlands
[d] Central Blood Institute, Research and Development Department, Blood Service Headquarters, Japanese Red Cross Society, Tokyo, Japan
[e] RIKEN BioResource Research Center, Cell Engineering Division, National Research and Development Corporation, Tsukuba, Japan

ARTICLE INFO

Keywords:
Nanoparticles
Hematopoietic stem and progenitor cells
CRISPR
Gene-editing
Sickle cell disease

ABSTRACT

Ex vivo gene editing of CD34$^+$ hematopoietic stem and progenitor cells (HSPCs) offers great opportunities to develop new treatments for a number of malignant and non-malignant diseases. Efficient gene-editing in HSPCs has been achieved using electroporation and/or viral transduction to deliver the CRISPR-complex, but cellular toxicity is a drawback of currently used methods. Nanoparticle (NP)-based gene-editing strategies can further enhance the gene-editing potential of HSPCs and provide a delivery system for *in vivo* application. Here, we developed CRISPR/Cas9-PLGA-NPs efficiently encapsulating Cas9 protein, single gRNA and a fluorescent probe. The initial 'burst' of Cas9 and gRNA release was followed by a sustained release pattern. CRISPR/Cas9-PLGA-NPs were taken up and processed by human HSPCs, without inducing cellular cytotoxicity. Upon escape from the lysosomal compartment, CRISPR/Cas9-PLGA-NPs-mediated gene editing of the γ-globin gene locus resulted in elevated expression of fetal hemoglobin (HbF) in primary erythroid cells. The development of CRISPR/Cas9-PLGA-NPs provides an attractive tool for the delivery of the CRISPR components to target HSPCs, and could provide the basis for *in vivo* treatment of hemoglobinopathies and other genetic diseases.

1. Introduction

β-hemoglobinopathies, such as sickle cell disease (SCD) and β-thalassemia, are the most common monogenic disorders caused by mutations in the β-globin gene which encodes two subunits of adult hemoglobin (HbA, $\alpha_2\beta_2$). SCD is caused by a single nucleotide substitution (glutamate to valine) in the codon for amino acid 6 that affects the shape of erythrocytes. Erythrocytes carrying sickle hemoglobin (HbS, two mutant β-globins with two α-globins) become rigid under low oxygen conditions and deform to the typical sickle shape [1]. These occlude small blood vessels, resulting in sickle cell crises, hemolytic crises, progressive tissue and organ damage, severe pain and strokes [2,3]. The only permanent cure is transplantation of healthy hematopoietic stem cells (HSCs) [4,5], but the treatment is risky and there is a shortage of suitable donors.

HSC gene therapy holds great promise as an alternative curative treatment for hemoglobinopathies. Disease symptoms are ameliorated by mimicking a benign mutation causing *hereditary persistence of fetal hemoglobin* (HPFH), where large deletions or point mutations in the β-globin locus prevent binding of γ-globin repressors [6]. In this approach, reactivated γ-globin associates with α-globin to form fetal hemoglobin (HbF, $\alpha_2\gamma_2$), which takes over the function of the mutated adult β-chains [7] (HbA,$\alpha_2\beta_2$). Several genetic strategies have been investigated to achieve induction of HbF in patient-derived HSPCs for autologous transplantation [8–19].

Clustered regularly interspaced palindromic repeats (CRISPR) genome-editing technology is a relatively new discovery, but has rapidly become a powerful strategy with great potential to cure a large variety of human diseases, including those of the hematopoietic system. CRISPR-based genome editing approaches targeting a specific region of the

* Corresponding author. Translational Nanobiomaterials and Imaging, Department of Radiology, Bldg.1, C2-192, Leiden University Medical Center, Albinusdreef 2, 2333, ZA, Leiden, the Netherlands.
E-mail address: c.eich@lumc.nl (C. Eich).

https://doi.org/10.1016/j.biomaterials.2020.120580
Received 21 July 2020; Received in revised form 16 November 2020; Accepted 23 November 2020
Available online 7 December 2020

γ-globin promoter to mimic a natural occurring HPFH-mutation were successfully applied *in vitro* and *ex vivo* in $CD34^+$ HSPCs to elevate HbF expression [20,21]. This chromosomal region recruits BCL11A, a powerful repressor of the γ-globin gene, which makes it an attractive therapeutic target. Recently, CRISPR genome-editing approaches of the same target led to persistent HbF reactivation after engraftment of edited, highly purified HSPCs in non-human primates [14].

The CRISPR ribonucleoprotein (RNP) complex, consisting of a short guide RNA (gRNA) to recognize target DNA and Cas9 endonuclease to introduce double-stranded breaks, can be introduced into cells by viral vectors encoding for Cas9 and gRNAs. Alternatively, gRNA and purified Cas9 protein can be delivered by biophysical methods including electroporation [14,22], lipids [23], iTOP [24], TRIAMF [19], nanoparticles [25,26] and cell-penetrating peptides [27]. Until now, viral vectors are the most commonly used carriers for the delivery of CRISPR/Cas9 to HSPCs in clinical applications. They allow for the selection and purification of edited cells; however, they carry the risk of random vector integration into the genome, are less efficient than purified RNP complexes and may induce cytotoxicity. To increase efficacy, most recent HSPC CRISPR-editing approaches utilize electroporation to deliver gRNA and Cas9 directly into target cells [14,22,28]. Both viral and electroporation-based CRISPR-genome editing approaches for hemoglobinopathies require *ex vivo* manipulation of HSPCs. This makes the treatment expensive and limits the number of patients who will have access once this new technology becomes available for treatment.

For a systemic therapeutic application for hemoglobinopathies, the CRISPR components would need to be co-delivered at sufficiently high concentrations inside HSPCs, potentially following mobilization of HSPCs into the blood. However, the CRISPR genome-editing components are prone to proteolytic degradation and possess a poor membrane permeability potential [29]. Thus, a delivery system that ensures high payload delivery towards HSPCs, thereby improving the ratio of efficacy/toxicity, would be advantageous.

Here, we utilized biodegradable and FDA-approved poly(lactic-co-glycolic acid) (PLGA)-NPs as delivery vehicles for the CRISPR/Cas9 complex. PLGA is one of the most successfully developed biodegradable polymers [30] with well described and adaptable methods of production. In addition, PLGA presents a stable linker to polyethylene glycol to improve the circulation and half-life in the blood and to couple targeting moieties for specific cellular uptake [30–33]. During NP-formulation, drugs, proteins, RNA, or imaging agents can be incorporated into the PLGA core. Finally, the PLGA core protects the payload from premature degradation [34].

In this study, CRISPR/Cas9-PLGA-NPs were successfully formulated and readily taken up by HUDEP-2 cells, primary erythroblasts and $CD34^+$ cells, shown to be non-toxic and to increase the levels of HbF significantly. The development of CRISPR/Cas9-PLGA-NPs to raise HbF levels in erythroid cells increases the toolbox of CRISPR/Cas9 delivery vehicles to target HSPCs for the treatment of hemoglobinopathies and could be adjusted to other genetic diseases.

2. Materials and methods

2.1. Materials

For the preparation of NPs, dichloromethane (DCM) and dimethylformamide (DMF) were purchased from Sigma-Aldrich® (Zwijndrecht, The Netherlands). Poly (D,L-Lactide-co-Glycolide) 50:50 (molecular weight 7000–17,000 Da), polyvinyl alcohol (PVA), calcium nitrate ($Ca(NO_3)_2$) and diammonium hydrogen phosphate ($(NH_4)_2HPO_4$) were purchased from Sigma-Aldrich. Cy5 Acid was purchased from Kerafast (Boston, US). Alt-R® Cas9 Nuclease V3 (*S. pyogenes*), Alt-R® CRISPR-Cas9 crRNA, Alt-R® CRISPR-Cas9 tracrRNA, Alt-R® CRISPR-Cas9 tracrRNA-ATTO™ 550 and nuclease-free water were purchased from Integrated DNA Technologies (IDT), (Iowa, US). Chemically modified sgRNAs were purchased from Biolegio (Nijmegen, The Netherlands). Lipofectamine™ CRISPRMAX™ Cas9 Transfection Reagent was purchased from ThemoFisher Scientific (Massachusetts, US).

For cell culture, StemSpan and MethoCult™ H4434 Classic medium were purchased from STEMCELL Technologies (Vancouver, Canada). EPO Eprex (1000IE) was purchased from Janssen-Cilag AG (Zug, Germany). Human recombinant SCF was purchased from BioLegend (San Diego, US). Dexamethasone, SyntheChol and doxycycline were purchased from Sigma Aldrich.

For flow cytometry, cells were stained with anti–HbF-FITC (clone REA533; Miltenyi Biotec, Bergisch Gladbach, Germany), anti–GPA (clone HIR2; BioLegend, California, US) and anti–CD71 (clone CY1G4, BioLegend). Unconjugated antibodies were detected with the secondary antibody goat anti-mouse IgG (H+L)-Alexa Fluor 488 (Invitrogen, ThermoFisher Scientific). For confocal microscopy, cells were stained with anti-GPA (BioLegend), anti-Cas9 (clone 7A9, BioLegend), anti-CD34 (clone 561, BioLegend) and anti-EEA-1 (polyclonal, Invitrogen, ThermoFisher Scientific). Secondary antibodies were donkey anti-rabbit Alexa-Fluor 488, goat anti-mouse IgG1 Alexa Fluor 488, goat anti-mouse IgG2a Alexa Fluor 488 and goat anti-mouse IgG1 Alexa Fluor 568 (Invitrogen, ThermoFisher Scientific). Lysosomes were labelled with LysoTracker™ Green (Invitrogen, ThermoFisher Scientific).

2.2. gRNAs

sgRNAs (Biolegio) were purchased as oligonucleotides. eGFP-targeting sgRNA: GGG CGA GGA GCU GUU CAC CG; γ-globin targeting sgRNA [21]: CTT GTC AAG GCT ATT GGT CA; scrambled sgRNA (Biolegio): CCC GCU CCU CGA CAA GUG GC.

2.3. CRISPR/Cas9-PLGA-nanoparticle preparation

CRISPR/Cas9-PLGA-NPs were formulated according to an oil-in-water (W1/O/W2) double emulsion solvent evaporation method [35,36] (Fig. 1B). Prior to formulation, beakers, spatulas, sonicator tip and magnetic stirrers were cleaned, decontaminated with RNAse-zap solution (Sigma) and rinsed with RNAse-free water. Firstly, we prepared a complex of Cy5-dye and Cas9-protein (1). To this end, we dissolved 0.1 mg Cy5 (acid) dye in 40 μL of RNAse free water and then added 66 μg of Cas9. The mixture was incubated for 30 min at room temperature (RT). Secondly, we prepared a solution of calcium phosphate to precipitate the gRNA (2). To this end, we modified a rapid precipitation method that was reported earlier [37]. We prepared two pipettes, one containing 105 μL of aqueous calcium nitrate (6.25 mM) and another one with 105 μL of aqueous di-ammonium hydrogen phosphate (3.74 mM). Both solutions were simultaneously pipetted and mixed on top of a paraffin sheet. The resulting calcium phosphate solution was added dropwise into an Eppendorf tube containing 12.8 μg sgRNA or hybridized crRNA-tracerRNA complex (according to the IDT user manual) in 40 μL of duplex buffer, while vortexing. The mix of sgRNA and salt was cooled on ice for 5 min. In the next step the calcium phosphate-CRISPR/Cas9-PLGA-NPs were formulated: 10 mg of PLGA were dissolved in 750 μL DCM (3). First, the 210 μL of calcium phosphate and gRNA prepared in step 2 were added. Secondly, the 40 μL of Cy5-Cas9-complex prepared in step 1 were added. The mixture of calcium phosphate-gRNA, Cy5-Cas9 and PLGA-polymer was immediately emulsified under sonication (Sonifier 250, ultrasonic tip Branson, Connecticut, US) using the following settings: 60 s sonication time, 50% duty cycle, output control: 4. During sonication, the mixture was kept on ice. Immediately after sonication, an aqueous phase (3000 μL), containing 30 mg of the emulsifier PVA, was added dropwise to the W1/O phase. Prior to use, the aqueous phase of PVA was dissolved in a water bath at 80 °C for 20 min and cooled to RT. The solution was immediately sonicated as described above. After sonication, DCM was removed under reduced pressure (200–600 mbar) in a rotary evaporator for ~2 min and the excess of PVA was removed by centrifugation (15 min at 14,800 rpm at 4° C). Following centrifugation, the NPs were washed three times with

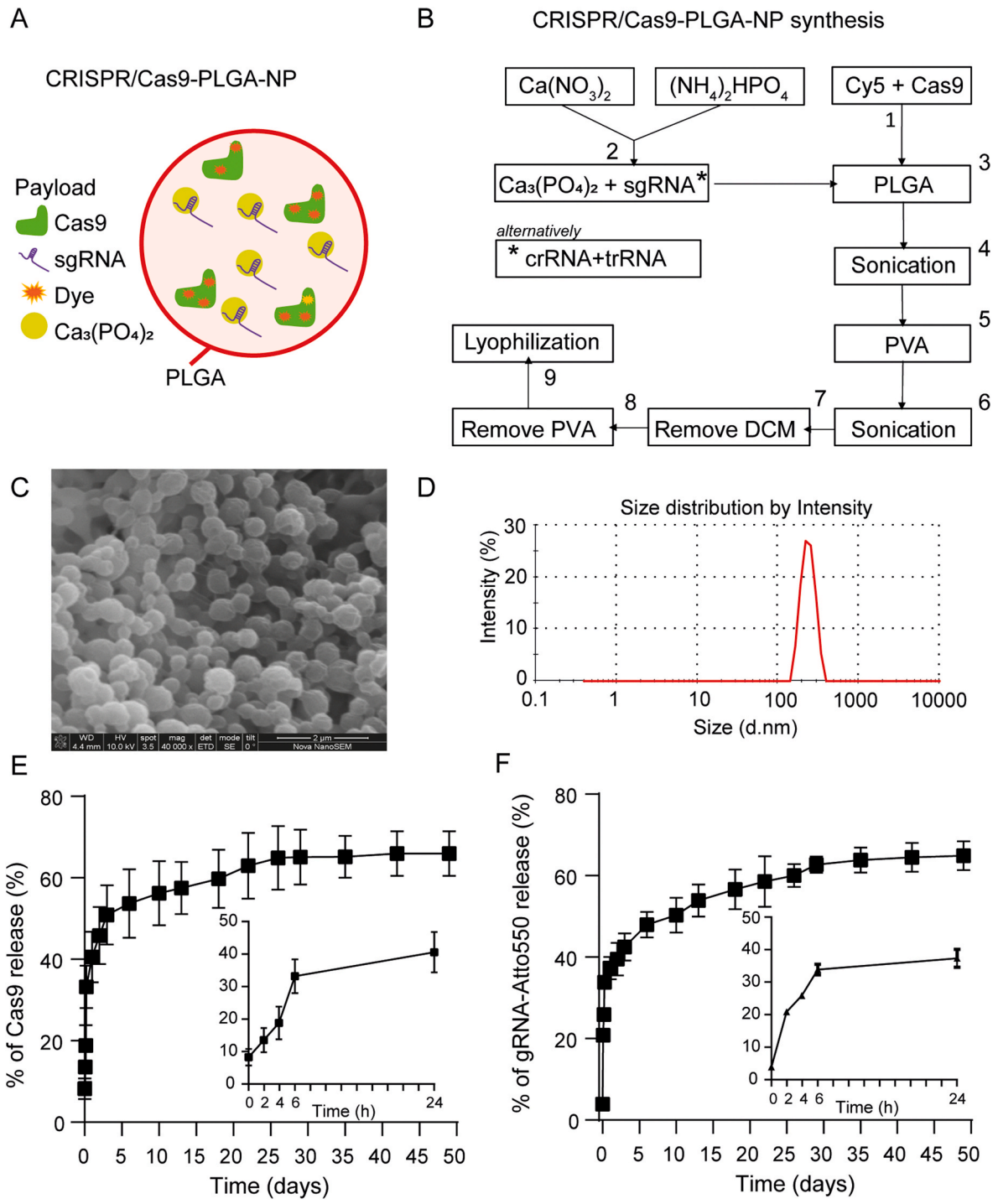

Fig. 1. Characterization of CRISPR/Cas9-PLGA-NPs. (A) Schematic representation of a CRISPR/Cas9-PLGA-NP made of polylactic-co-glycolic acid (PLGA). The CRISPR-components were encapsulated in form of guide RNA (single or hybridized gRNA) and purified Cas9 (*S.pyogenes*) protein. In addition, the NPs were equipped with a fluorescent dye (acid Cy5). (B) Schematic overview of the CRISPR/Cas9-PLGA-NP synthesis protocol using a double emulsion solvent evaporation method. (C) Representative scanning electron microscopy image of a CRISPR/Cas9-PLGA-NP formulation. Scale bar = 2 μm. (D) Representative dynamic light scattering measurement of a CRISPR/Cas9-PLGA-NP formulation. The average size of the NPs was 350–400 nm in diameter. Release kinetic studies of (E) Cas9 and (F) Atto-550-labelled gRNA from CRISPR/Cas9-PLGA-NPs in PBS pH 7.4 at 37 °C. Insets represent the kinetic release curve over the first 24 h. At the indicated time-points, release medium was collected and gRNA and Cas9 levels were quantified by spectrophotometer and nanodrop measurements, respectively. Results show representative release kinetic curves.

1000 μL RNAse-free water and subsequently freeze-dried. All washing solutions were stored to determine the loading efficacy of Cas9, Cy5 and gRNAs. The NPs were stored at −80 °C and rehydrated prior use.

2.4. Physicochemical characterization of CRISPR/Cas9-PLGA-NPs

Z-average size, polydispersity index (PDI) and zeta potential of CRISPR/Cas9-PLGA-NPs were measured using a Malvern ZetaSizer 2000 (Malvern, UK; software: ZetaSizer 7.03). Fixed scattering angle of 90° at

633 nm was set up for the analysis. DLS and zeta potential measurements were performed on CRISPR/Cas9-PLGA-NPs resuspended in RNAse-free water before freeze-drying.

2.5. Scanning electron microscopy

Surface morphology and homogeneity of CRISPR/Cas9-PLGA-NPs were observed by scanning electronic microscopy (SEM) using a Nano-SEM 200 microscope (FEI, Japan). The materials were coated with an ultrathin layer (300 Å) of Pd/Pt in an ion sputter coater (Cressington 208HR, United Kingdom).

2.6. Transmission electron microscopy

PLGA-NP shape and morphology were further characterized by transmission electron microscopy (TEM). To improve adherence of PLGA-NPs to the carbon-coated grids (Formvar/Carbon on 200 Mesh Copper; AGS162; Van Loenen Instruments; Zaandam, the Netherlands), 5 μL of 100 mg/mL poly-L-lysine hydrobromide (P1274-25 MG; Sigma-Aldrich; Zwijndrecht, the Netherlands) in PBS were pipetted onto each grid and incubated for 10 min. Subsequently, excess liquid was discarded by blotting onto a filter paper. Next, 3 μL of sample solution were applied onto the freshly coated grid and allowed to adhere for 1 min. Afterwards, excess sample was blotted onto a filter paper and 3 μL of filtered 2% uranyl acetate in distilled water were applied to the grid for negative staining of the sample. After 1 min, excess uranyl acetate was removed by blotting and the sample was air-dried for 10 min. Grids were mounted and examined using a Tecnai 12 Twin (FEI Company; Oregon, USA) equipped with an OneView Camera Model 1095 (Gatan; Pleasanton, USA) at a voltage of 120 kV. Digital images were acquired and stored using DigitalMicrograph 3.4 (Gatan).

2.7. Quantification of loading efficacy into CRISPR/Cas9-PLGA-NPs

Cy5 loading efficacy into CRISPR/Cas9-PLGA-NPs was indirectly determined by quantifying Cy5 in the supernatants of the washing steps collected during NP-preparation, using a spectrofluorometer, plotted against a Cy5 standard curve of known concentrations.

To quantify the amount of encapsulated gRNA, we prepared CRISPR/Cas9-PLGA-NPs encapsulating Cas9 and a hybridized gRNA consisting of crRNA and Atto550-labelled tracerRNA. gRNA loading efficacy into CRISPR/Cas9-PLGA-NPs was indirectly determined by quantifying the gRNA content in the supernatant of the washing steps collected during NP preparation. Supernatants and a standard curve of crRNA-tracerRNA-Atto550 with known concentrations were measured using a spectrofluorometer.

Cas9 loading efficacy into CRISPR/Cas9-PLGA-NPs was determined by nanodrop measurement. To this end, the amount of Cas9 protein in the supernatant of the washing steps collected during NP preparation was quantified. Per batch of NPs (10 mg PLGA), 66 μg Cas9 were added during formulation. Due to the low concentration of Cas9 in the collected washing solutions, we first pooled all washing solutions and concentrated the volume to 100 μL using Amicon® Ultra-2 Centrifugal Filters with a molecular weight cut-off of 100.000 kDa (Sigma Aldrich). The concentrated washing solutions were measured using a nanodrop at 280 nm and blanked against washing solutions of control NPs. Successful encapsulation of Cas9 was further confirmed by SDS and Western Blot analysis of CRISPR/Cas9-PLGA-NPs hydrolysed overnight with 0.8 M NaOH at 37 °C.

2.8. In vitro release kinetics of Cas9 and gRNA

To follow *in vitro* Cas9 and gRNA release, CRISPR/Cas9-PLGA-NPs encapsulating Cas9 and gRNA-Atto550 were resuspended in PBS at a concentration of 3.5 mg/mL. 300 μL of NP-solution (in triplicate) were placed in an Eppendorf tube and incubated at 37 °C on a heating block in shaking mode (400 rpm). At the indicated timepoints (0 h, 2 h, 4 h, 6 h, 24 h, 48 h, 96 h, 6 d, 10 d, 13 d, 18 d, 22 d, 26 d, 29 d, 35 d, 42 d and 49 d), 150 μL sample was withdrawn and the volume was replaced with 150 μL fresh PBS. After collecting the final timepoint, the samples and a gRNA-Atto550 standard curve were first measured using a spectrophotometer to quantify the amount of released gRNA. Next, the samples were concentrated to a volume of 20 μL using Amicon® Ultra-2 Centrifugal Filters and the amount of released Cas9 was determined by nanodrop measurement.

The cumulative release was calculated according to equation (1):

$$E(\%) = \left(V_E \sum_{1}^{n-1} C_i + V_0 C_n\right) \Big/ m_0 \times 100 \quad (1)$$

where E (%) is the cumulative release, V_E is the withdrawn volume, V_0 is the begin volume, C_i and C_n are the Cas9 or gRNA concentrations, $_i$ and $_n$ are the sampling times and m_0 is the total amount of Cas9 or gRNA loaded into CRISPR/Cas9-PLGA-NPs.

2.9. Cell culture

Human umbilical cord blood-derived erythroid progenitor-2 (HUDEP-2) were cultured as described previously [38]. Briefly, HUDEP-2 cells were cultured in StemSpan (Stem Cell Technologies) serum-free expansion medium supplemented with 1 μM dexamethasone, 1 μg/mL doxycycline, 50 ng/mL human SCF, 2 units/mL EPO, 0.4% SyntheChol and 1% penicillin–streptomycin. Differentiation of HUDEP-2 cells was initiated by removal of doxycycline, dexamethasone and SCF, and an increase in EPO to 10 units/ml. HUDEP-2-eGFP expressing cells were generated by lentiviral transduction of HUDEP-2 cells with pRRL-CMV-GFP plasmid (kind gift of M.J.W.E. Rabelink, LUMC). One week after transduction, eGFP-high-expressing HUDEP-2 cells were sorted using a BD (New Jersey, US) FACSARIA I flow cytometer and the bulk of eGFP-expressing cells was further propagated. As positive control in γ-globin targeting experiments, the gRNA/Cas9 RNP complex was delivered to WT HUDEP-2 cells by electroporation using the Neon transfection system (ThermoFisher Scientific). The following settings were used during electroporation: 1600 V, 10 ms, 3 pulses. Electroporated HUDEP-2 were propagated and used as control.

Peripheral blood mononuclear cells (PBMCs) were obtained from healthy buffy coat donors (Sanquin blood bank, The Netherlands) and were cultured according to a three-phase erythroid differentiation protocol in StemSpan serum-free expansion medium supplemented with 1 μM dexamethasone, 50 ng/mL human SCF, 2 units/mL EPO, 0.4% SyntheChol, and 1% penicillin–streptomycin [39,40]. During phase 1 (day 1–7), 1 ng/mL human interleukin (IL)-3 (BioLegend) and 40 ng/mL human insulin-like growth factor I (IGF) (BioLegend) were included. Phase 2 (days 8–12) included the same medium, except that IL-3 and IGF1 were withdrawn. Erythroid differentiation was monitored by flow cytometry using anti-CD71 and anti-GPA antibodies.

2.10. CRISPR/Cas9-PLGA-NPs-mediated gene editing

1×10^5 HUDEP-2 cells were resuspended in 100 μL StemSpan medium (including supplements) and plated into a 96-well (flat bottom) plate. Lyophilized CRISPR/Cas9-PLGA-NPs were resuspended at 5 mg/mL in RNAse-free water and immediately further diluted in StemSpan medium. Prior to use, CRISPR/Cas9-PLGA-NPs were kept at all time on ice. 100 μL of CRISPR/Cas9-PLGA-NPs were added to 100 μL of HUDEP-2 cells to reach a final concentration of 200 μg/mL, 100 μg/mL, 50 μg/mL, 25 μg/mL or 12.5 μg/mL. HUDEP-2 cells were incubated with CRISPR/Cas9-PLGA-NPs or control-NPs for 24 h at 37 °C, subsequently excessive NPs were washed away with fresh medium. NP-treated HUDEP-2 were cultured up to 21 days after NP-treatment. The cells were split and the medium was refreshed every three days. At designated

timepoints, cells were withdrawn for flow cytometry and RNA analysis. Samples were prepared in triplicate.

Primary erythroblasts were edited at the end of phase 1 using the erythroid differentiation protocol. At day 8, when the cell culture was populated by erythroid progenitors, the cells were collected and 1×10^5 cells were resuspended in 100 μL phase 2-medium, plated into a 96-well (flat bottom) plate and treated with 200 μg/mL, 100 μg/mL, 50 μg/mL, 25 μg/mL or 12.5 μg/mL CRISPR/Cas9-PLGA-NPs or control-NPs, as described above. The cells were expanded and cultured in phase-2 medium until day 21. At designated timepoints, cells were withdrawn for flow cytometry and RNA analysis.

2.11. Flow cytometry

HUDEP-2 cells, primary erythroblasts or isolated $CD34^+$ cells were collected and washed in PBS. To assess cell viability after NP-treatment, cells were resuspended in FACS buffer (2.5 g BSA in 500 mL PBS, 0.02% sodium azide) containing Hoechst. The percentage of Hoechst positive/negative cells was assessed using a BD LSR-II equipped with a UV-laser. NP-uptake was assessed by measuring the percentage of Cy5-positive cells compared to non-treated control cells.

To determine the expression of HbF in HUDEP-2 cells or primary erythroblasts, cells were fixed, permeabilized and stained using an intracellular labelling kit (Inside Stain Kit, Miltenyi Biotec) and anti-HbF-Fitc antibody (Miltenyi Biotec) according to manufactures instructions.

2.12. Confocal microscopy

Uptake and intracellular routing of CRISPR/Cas9-PLGA-NPs in HUDEP-2 cells were analysed by confocal microscopy. To this end, HUDEP-2 cells were incubated with 200 μg/mL CRISPR/Cas9-PLGA-NPs for 1 h, 4 h and 24 h at 37 °C and subsequently washed in PBS. The cell membrane was labelled with 10 μg/mL anti-GPA primary antibody, followed by detection by a secondary antibody. After labelling, the cells were fixed with 4% paraformaldehyde (PFA) in PBS for 15 min at RT, washed and permeabilized with 0.1% Triton in PBS for 5 min. Intracellular labelling was performed by incubating the cells with 10 μg/mL anti-EEA-1 or anti-Cas9 antibody, followed by incubation with a conjugated secondary antibody. Cells were washed and seeded on cover slips coated with 100 μg/mL poly-L-Lysine (Sigma Aldrich) for 15 min at RT. Finally, the cells were labelled with DAPI for 5 min at RT, fixed in 1% PFA for 15 min and embedded in mounting medium containing Mowiol and Dabco (Sigma Aldrich). For labelling of lysosomes, cells were extensively washed and incubated with green lysotracker (ThermoFisher Scientific) for 30 min at 37 °C prior to cell membrane labelling. Cas9 encapsulated inside CRISPR/Cas9-PLGA-NPs was detected by anti-Cas9 labelling. Briefly, control-NPs (without Cas9) and CRISPR/Cas9-PLGA-NPs were immobilized on poly-L-Lysine-coated cover-slips (100 μg/mL), fixed for 10 min with 4% PFA, washed and subsequently labelled with 10 μg/mL anti-Cas9 antibody. The NPs were washed and labelled with an AF488 conjugated anti-mouse secondary antibody. All labelling and washing steps were performed in PBS containing 0.5% saponin (SIGMA). The NPs were embedded in mounting medium containing Mowiol and Dabco. Fluorescence imaging was performed with a SP5 confocal microscope (Wetzlar, Germany) using a 63× oil objective.

2.13. RT-qPCR

Edited HUDEP-2 and control cells were washed with PBS and lysed in the cell culture plate using TRIzol (Invitrogen, Grand Island, NY, USA). Total RNA content was isolated according to manufacturer's protocol. Reverse transcription was performed using the M-MLV Reverse Transcriptase (Promega, Madison, WI, USA). Expression levels of *GAPDH*, *EGFP, HBB and HBG* were analysed using real-time, quantitative PCR. All real-time PCR reactions were performed using the Real-Time PCR Detection System from Biorad and all amplifications were performed using SYBR Green and PlatinumTaq (Thermofisher Scientific). The quality of the products was confirmed by melting curve analysis. The following expression primers were used: forward (F) primer CATTGCCCTCAACGACCACT and reverse (R) primer GGTGGTCCAGGGGTCTTACT for *GAPDH*, F primer GCCCTGGCCCACAAGTATC and R primer GCCCTTCATAATATCCCCCAGTT for *HBB*, F primer GGTGACCGTTTTGGCAATCC and R primer GTATCTGGAGGACAGGGCAC for *HBG,* F primer ATCTTCTTCAAGGACGACGG and R primer GGCTGTTGTAGTTGTACTCC for *EGFP*. Throughout this work, percent *HBG* mRNA refers to the abundance of *HBG* mRNA expressed relative to the sum of the abundance of γ-globin and β-globin transcripts ([*HBG*/(*HBB* + *HBG*]*100).

2.14. Methylcellulose

Methylcellulose colony-forming assay was performed as described previously [41]. $CD34^+$ were isolated from PBMCs using human $CD34^+$ MicroBeadKit (Miltenyi) and MS columns for positive selection of $CD34^+$ cells. Isolated $CD34^+$ cells were incubated with 200 μg/mL CRISPR/Cas9-PLGA-NPs or control-NPs in IMDM medium for 30 min at 37 °C, 5% CO_2. Subsequently, the cells were centrifuged and (without washing) seeded in methylcellulose. Per dish, 500 $CD34^+$ cells were seeded in triplicate in methylcellulose (1 mL per dish; H4434; Stem Cell Technologies) containing 1% PS and incubated for 14 days at 37 °C, 5% CO_2. Colonies were characterized and counted with a bright field microscope, and the Cy5 signal inside the colonies was obtained in a scan with the Odyssey imaging system (LI-COR, Nebraska, US) at 680 nm.

2.15. Sanger sequencing and TIDE analysis

Sanger sequencing was performed on BFU-E colonies grown for 14 days in methylcellulose. After characterization and counting, BFU-E colonies were harvested in a 96-well plate and washed with PBS. Subsequently, DNA was extracted using the Wizard Genomic DNA Purification Kit (Promega). 2 μL of the cell lysate was used as input in a PCR reaction using Phusion DNA polymerase (ThermoFisher Scientific) and the following primers: F ACGGCTGACAAAAGAAGTCC and R GGGTTTCTCCTCCAGCAT. PCR products were purified using Wizard SV Gel and PCR clean-up system (Promega). TIDE analysis was performed on Sanger sequencing trace data to access indel frequency in BFU-E colonies using the online tool http://shinyapps.datacurators.nl/tide/ [42].

3. Results

3.1. CRISPR/Cas9-PLGA-NPs synthesis and characterization

To circumvent efficacy and safety issues of viral vehicles, we designed PLGA-NPs encapsulating Cas9 (*S.pyogenes*) protein, gRNA and the fluorescent dye Cy5 (Fig. 1A). The aim of this study was to synthesize a delivery vehicle for CRISPR/Cas9 that is efficiently processed by HSPCs and could be monitored by fluorescence microscopy. In the classical solvent evaporation technique, gRNAs can easily escape from the encapsulation process due to their low molecular weight, hydrophilicity and the electrostatic repulsion between the phosphate backbone of the RNA and the carboxylic acid end groups of the PLGA-building blocks [43]. To avoid this, we adjusted a previously reported method where siRNA absorbed onto the surface of calcium phosphate was encapsulated into the hydrophobic core of PLGA [37].

Here, we synthesized CRISPR/Cas9-PLGA-NPs according to an oil-in-water double emulsion solvent evaporation method (Fig. 1B). Prior to encapsulation, we prepared a complex of Cy5 acid (net charge −1) and Cas9 (net charge of +22), based on electrostatic interaction (Fig. 1A and B). Cy5 acid dye contains a non-activated carboxylic acid; thus, the molecule is considered non-reactive. We reasoned that forming a

complex between Cas9 and Cy5 instead of directly conjugating Cy5 to the Cas9 protein would avoid loss of Cas9 functionality and increase the encapsulation efficacy of the Cy5 dye. Secondly, we prepared a solution of calcium phosphate to precipitate the gRNA (sgRNA or hybridized crRNA-tracerRNA complex) under formation of calcium phosphate/gRNA complexes. In the next step we synthesized calcium phosphate-CRISPR/Cas9-PLGA-NPs: PLGA was dissolved in DCM and then the calcium phosphate/gRNA- and Cas9/Cy5-in-water complexes were added. Sonication led to the formation of the first emulsion with calcium phosphate/gRNA and Cas9/Cy5 complexes in-water in the oil phase. Addition of PVA (dissolved in water) and subsequent sonication led to the formation of a stable double oil-in-water emulsion. The organic solvent was removed under reduced pressure and the surfactant PVA under centrifugation. The resulting NPs were immediately freeze-dried.

We first encapsulated chemically modified gRNA directed against the sequence of enhanced green fluorescent protein (eGFP) or a scrambled control sequence. The spheric morphology of the NPs was confirmed by SEM (Fig. 1C) and the size of the NPs was determined by dynamic light scattering (DLS) analysis as ~370 nm in diameter (Table 1, Fig. 1D) and the polydispersity index (PDI) values of 0.1–0.2 obtained from the DLS measurement indicated a homogeneous size distribution (Table 1). In addition, ZetaSizer measurement showed a negative surface charge of the NPs (Table 1). In contrast to control NPs without Cas9, encapsulation of Cas9 increased the size of the NPs from 215 to >300 nm (Table 1), indicating successful encapsulation of Cas9. Nanodrop analysis of the washing solutions generated during NP synthesis showed encapsulation efficacies of 49–75% for Cas9 and 69–89% for sgRNA. In addition, spectrophotometry measurements revealed that 26–65% of Cy5 dye was encapsulated (Table 1).

To monitor the release kinetics of Cas9 from CRISPR/Cas9-PLGA-NPs, we incubated the NPs in PBS at 37 °C for 49 days and withdrew samples at designated timepoints. The amount of Cas9 was measured by nanodrop and the cumulative release was calculated (Fig. 1E). The gRNA release was calculated from a batch of CRISPR/Cas9-PLGA-NPs that encapsulated Atto-550-labelled gRNA (Fig. 1F). The release kinetic studies showed that 35% of the encapsulated gRNA and 40% of the Cas9 were rapidly released within the first 24 h. This was followed by a period of sustained release, which flattened out and reached a plateau profile at approximately day 30, lasting until the end of the analysis (Fig. 1E and F). DLS and Zeta potential measurements did not show significant changes in size and surface charge over a period of 7 weeks at 37 °C (Supplementary Fig. 1A and B). In addition, TEM analysis of the NPs showed no changes in NP structure at the analysed timepoints (up to 5 weeks) (Supplementary Fig. 1C). To draw conclusions on whether the remaining CRISPR components were trapped inside the PLGA core, the CRISPR/Cas9-PLGA-NPs were labelled with anti-Cas9 antibody at timepoint 0, and after 3 and 5 weeks of incubation at 37 °C (Supplementary Fig. 1D). The Cas9 labelling coincided with the signal of the Cy5 fluorescent dye that was co-encapsulated together with the CRISPR components inside the PLGA core. The signal decreased over time, but Cas9 could still be detected in the NPs after 3–5 weeks at 37 °C, indicating that the release of Cas9 from PLGA-NPs was incomplete.

Table 1
Physico-chemical characterization of distinct NP-batches. PDI = polydispersity index; EE = encapsulation efficacy.

Sample	NP size ± S.D. (nm)	Zeta Potential ± S.D. (mV)	PDI	EE (%) gRNA	EE (%) Cas9	EE (%) Cy5
PLGA-NP-(sgRNA, Cy5)	214.7 ± 3.06	−16.0 ± 1.79	0.22 ± 0.05	83.85	–	26.29
PLGA-NP-(Cas9, "scrambled sgRNA", Cy5)	378.5 ± 79.37	−17.6 ± 2.17	0.12 ± 0.05	84.58	49.12	47.39
PLGA-NP-(Cas9, "eGFP-sgRNA", Cy5)	362.4 ± 46.68	−25.4 ± 4.4	0.21 ± 0.05	88.91	70.91	64.78
PLGA-NP-(Cas9, "eGFP-crRNA + tracerRNA", Cy5)	307.67 ± 2.45	−13.8 ± 1.42	0.23 ± 0.14	78.52	75.01	32.63
PLGA-NP-(Cas9, "γ-globin targeting sgRNA", Cy5)	296.67 ± 101.04	−9.49 ± 0.9	0.15 ± 0.06	69.92	75.17	60.68

3.2. Evaluation of toxicity and uptake of CRISPR/Cas9-PLGA-NPs

Next, we assessed potential toxicity of CRISPR/Cas9-PLGA-NPs on the human erythroblast cell line HUDEP-2. HUDEP-2 cells were incubated for 24 h with increasing concentrations of CRISPR/Cas9-PLGA-NPs and cell viability was assessed by flow cytometry on day 3, 6, 9 and 13 after NP-uptake (Fig. 2A). The NPs did not induce cytotoxic effects, even at a concentration of 200 μg/mL. Next to cell viability, we also measured NP-uptake by flow cytometry by determining the percentage of Cy5-positive HUDEP-2 cells. Quantification of the Cy5 signal on day 3 post NP-uptake showed that CRISPR/Cas9-PLGA-NPs were readily taken up HUDEP-2 cells in a concentration dependent-manner (Fig. 2B). At day 6, the Cy5 signal greatly decreased, indicating that the payload diffused out of the CRISPR/Cas9-PLGA-NPs at this time point.

We further analysed the intracellular routing of CRISPR/Cas9-PLGA-NPs by confocal microscopy. To this end, HUDEP-2 cells were incubated with 100 μg/mL CRISPR/Cas9-PLGA-NPs for 1 h, 4 h and 24 h and subsequently labelled for the endosomal marker EEA-1 or incubated with lysotracker. In line with the flow cytometry data, HUDEP-2 cells had readily taken up NPs (Fig. 2C and D). Visual inspection revealed that 1 h after uptake the CRISPR/Cas9-PLGA-NPs preferentially colocalized with endosomes, and 4 h after uptake with lysosomes. Quantification of the Manders colocalization coefficient of the Cy5 signal from the NPs and EEA-1 confirmed a significantly higher colocalization 1 h after NP uptake, compared to 24 h (Fig. 2E). In contrast to EEA-1, colocalization with lysosomes increased after 4 h, and then decreased after 24 h (Fig. 2F). Our data suggests an increasing exclusion of NPs from the endosomal/lysosomal routing and translocation to the cytosol within 24 h after uptake. Furthermore, labelling of Cas9 revealed that shortly after NP-uptake, Cas9 expression overlapped with Cy5, but after 24 h Cas9 and Cy5 expression appeared diffuse (Supplementary Fig. 2), indicating that a fraction of Cas9 diffused out of NPs within 24 h after cellular uptake.

3.3. Proof-of-concept: CRISPR/Cas9-PLGA-NP functionality

Next, we analysed the functionality of CRISPR/Cas9-PLGA-NPs. We generated eGFP-expressing HUDEP-2 cells by lentiviral transduction followed by bulk sorting of eGFP-positive cells to test the encapsulated eGFP-targeting sgRNA and Cas9. HUDEP-2-eGFP cells were incubated with increasing concentrations of CRISPR/Cas9-PLGA-NPs or control-NPs (Cas9, Cy5 and scrambled gRNA) and the bulk of NP-treated HUDEP-2 cells was propagated (Fig. 3A and B). At day 3, 6, 9 and 13 eGFP expression was measured by flow cytometry. eGFP protein expression was slightly reduced as early as 3 days after NP-uptake, compared to control-NPs, and showed significant reduction in eGFP signal on day 6 and day 9 after NP-uptake. On day 13, eGFP-expression was reduced by 70%, which was confirmed by reduction of *EGFP* mRNA levels (Fig. 3C), thus demonstrating the functionality of CRISPR/Cas9-PLGA-NPs. We wondered whether gene editing would be as efficient when encapsulating a hybridized gRNA consisting of cr and tracer RNA instead of a sgRNA. To this end, we prepared a batch of CRISPR/Cas9-PLGA-NPs with eGFP-targeting hybridized gRNA (Table 1) and

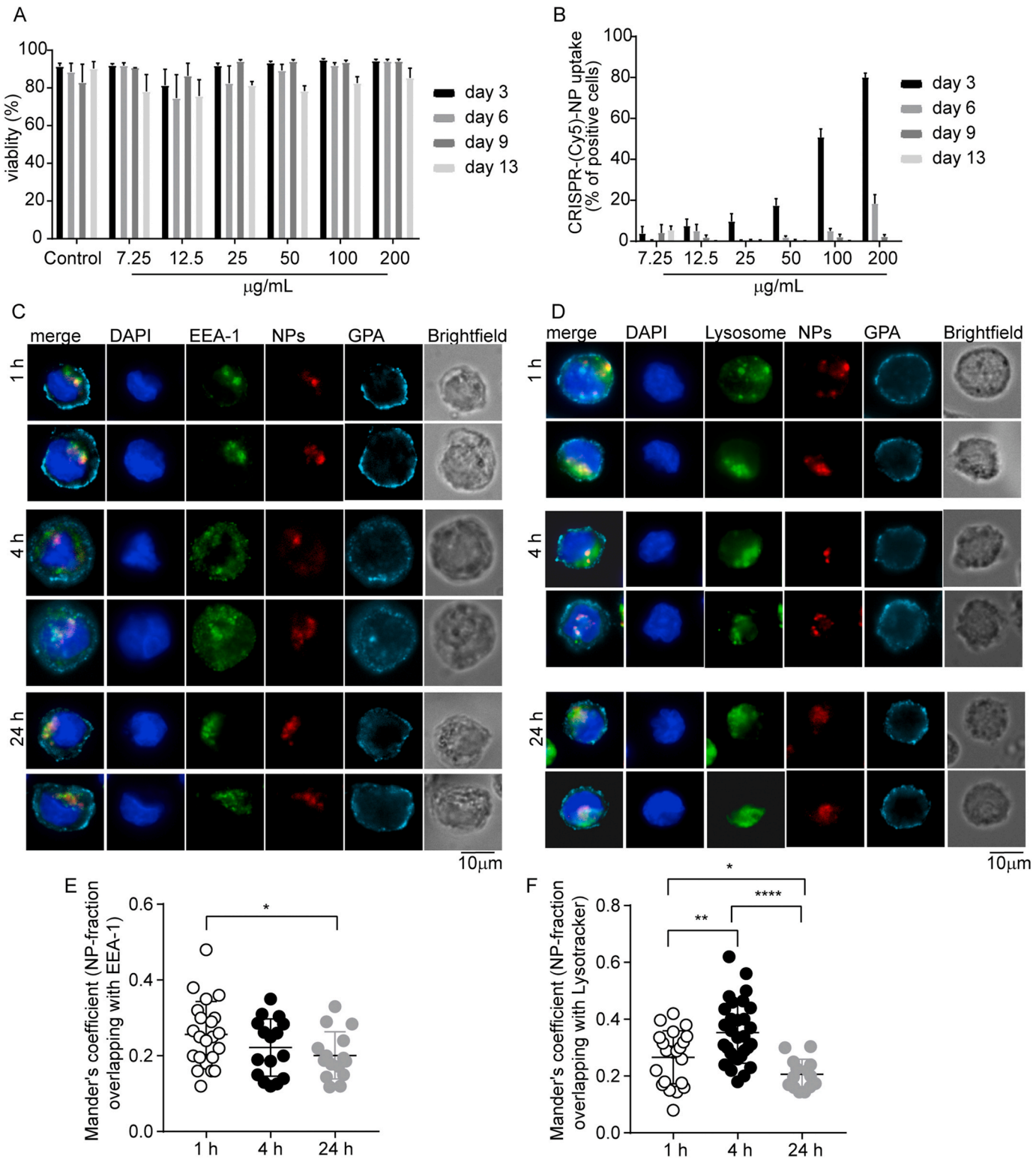

Fig. 2. Uptake and intracellular routing of CRISPR/Cas9-PLGA-NPs in hematopoietic cells. (A) Viability of HUDEP-2 at day 3, 6, 9 and 13 after incubation with various concentrations of CRISPR/Cas9-PLGA-NPs and control-NPs, determined by flow cytometry as Hoechst-negative cells. (B) % of $Cy5^{+}$ cells at day 3, 6, 9 and 13 after NP-uptake, measured by flow cytometry (C–D) Representative pictures of the intracellular routing of CRISPR/Cas9-PLGA-NPs analysed by confocal microscopy. Uptake of CRISPR/Cas9-PLGA-NPs (red) by HUDEP-2 cells 1, 4 and 24 h after incubation with 100 µg/mL of NPs. Cells were fixed and stained with DAPI (nucleus = blue), the cell surface marker GPA (cyan) and (C) the early endosomal marker EEA-1 or (D) with lysotracker (green). Scale bar = 10 µm. Colocalization between (E) NPs and EEA-1 or (F) NP and lysotracker as determined by the Mander's coefficients (M1). Results are representative of multiple cells in two independent experiments All P-values were generated using Mann-Whitney test. *=< p 0.476, ****=< p 0.0001. (For interpretation of the references to colour in this figure legend, the reader is referred to the Web version of this article.)

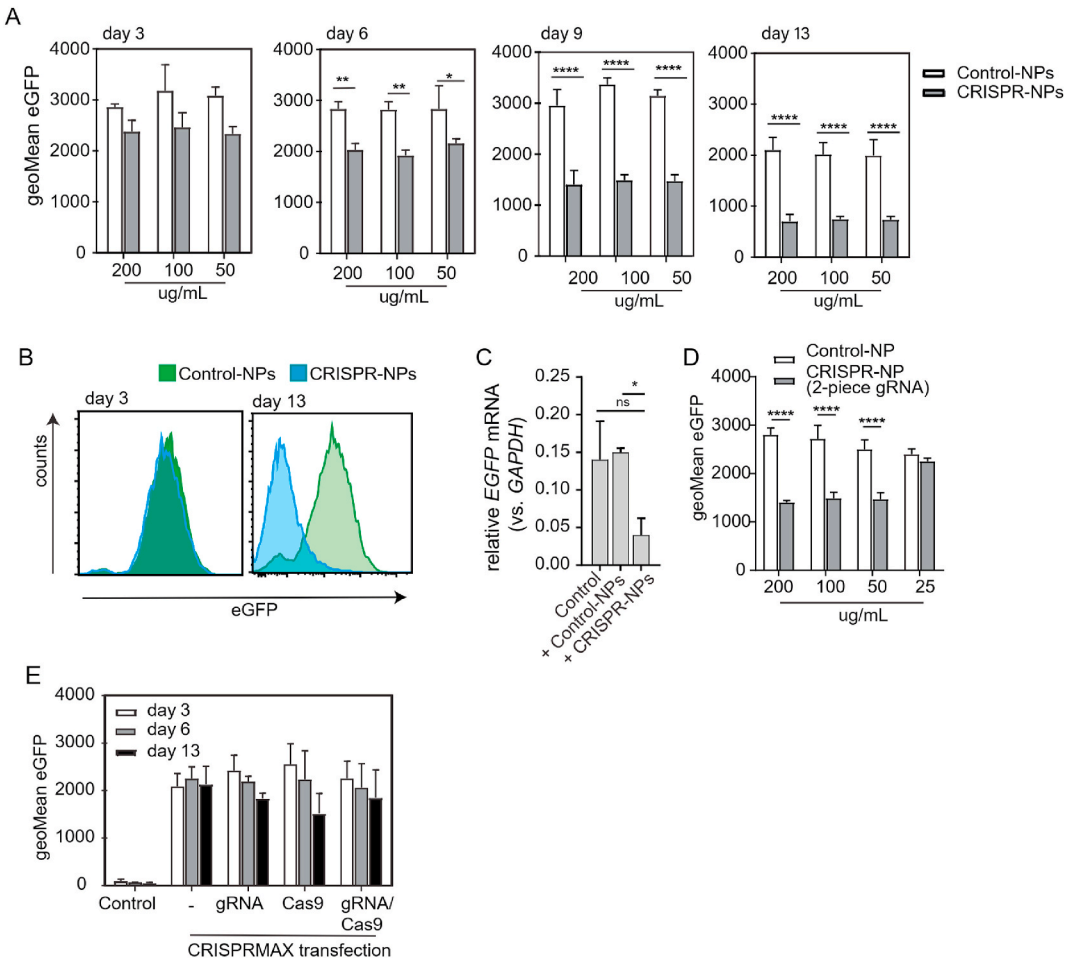

Fig. 3. Gene-editing by CRISPR/Cas9-PLGA-NPs. (A) eGFP-expressing HUDEP-2 cells were incubated with 50, 100 and 200 μg/mL CRISPR/Cas9-PLGA-NPs, encapsulating a sgRNA to disrupt the *EGFP* gene, and followed up to day 13 after NP-incubation by flow cytometry. (B) Representative flow cytometry data of eGFP-expressing HUDEP-2 cells, treated with control and CRISPR/Cas9-PLGA-NPs, at day 3 and day 13 after NP-treatment. (C) relative *EGFP* mRNA expression (vs *GAPDH*) in control HUDEP-2-eGFP cells and CRISPR/Cas9-NP-treated cells, measured by RT-qPCR on day 11 post NP-incubation. (D) eGFP-expressing HUDEP-2 cells were incubated with 50, 100 and 200 μg/mL CRISPR/Cas9-PLGA-NPs, encapsulating hybrid gRNA consisting of crRNA and tracer RNA. Cells were analysed on day 13 after NP-incubation by flow cytometry. (E) Gene-editing of HUDEP-2-eGFP cells using lipofection (CRISPRMAX). Cells were analysed on day 3, 6, and 13 post RNP-complex transfection. Data represent the mean ± SEM of 5 independent experiments. All P-values were compared to the respective control cells using Mann-Whitney test. *=< p 0.0338, **=< p 0.0068, ****=< p 0.001.

evaluated the functionality on eGFP-expressing HUDEP-2 cells on day 13 after NP-treatment (Fig. 3D). The gene-editing efficacy of the hybridized gRNA was comparable to the sgRNA, resulting in 50% reduction in eGFP-signal compared to control-NPs. To evaluate the efficacy of CRISPR/Cas9-PLGA-NPs compared to other non-viral delivery methods, we transfected eGFP-expressing HUDEP-2 cells with Cas9 and gRNA (eGFP) using lipofection (Fig. 3E). We did not observe any reduction in eGFP-expression when using lipofection-mediated delivery of the CRISPR-RNP complex, demonstrating the efficacy of CRISPR/Cas9-PLGA-NPs as alternative delivery system for the RNP complex in erythroblasts.

3.4. CRISPR/Cas9-PLGA-NP as delivery vehicle for therapeutic gRNAs

To evaluate the efficacy of CRISPR/Cas9-PLGA-NPs for therapeutic purposes, we prepared CRISPR/Cas9-PLGA-NPs encapsulating a sgRNA that efficiently induces a deletion within the γ-globin promoter, which abolishes binding of HbF transcriptional repressors, leading to clinically significant upregulation of HbF expression in erythroid cells (Table 1) [21]'. WT HUDEP-2 cells were treated with CRISPR/Cas9-PLGA-NPs and control-NPs. CRISPR/Cas9-PLGA-NPs targeting the γ-globin promoter region did not compromise cell viability, monitored at day 13 post NP-treatment by flow cytometry (Supplementary Fig. 3A). HUDEP-2 cell morphology was not affected by treatment with CRISPR/Cas9-PLGA-NPs (Supplementary Fig. 3B), nor did the NPs induce differentiation (Supplementary Fig. 3C).

Next, we incubated HUDEP-2 cells with CRISPR/Cas9-PLGA-NPs and evaluated the percentage of HbF-positive (F) cells by flow cytometry at day 13 after NP-treatment (Fig. 4A). 200 μg/mL or 100 μg/mL CRISPR/Cas9-PLGA-NPs increased the percentage of F-cells (50.6% and 70.4%, respectively), compared to 200 μg/mL of control-NPs encapsulating scrambled gRNA (8.2%) or electroporation of Cas9 and the same sgRNA (24.7%).

Flow cytometry results were validated by RT-PCR (Fig. 4B–D). 13 days after NP-incubation, the levels of adult β-globin (*HBB*) mRNA transcript were reduced in the electroporation control and upon treatment with CRISPR/Cas9-PLGA-NPs, in a concentration dependent-manner (Fig. 4B) and the levels of γ-globin (*HBG*) mRNA transcript increased accordingly (Fig. 4C). In electroporated cells, the percentage of γ-globin mRNA increased to 29%, while CRISPR/Cas9-PLGA-NPs raised the percentage of γ-globin to 47–69%, compared to 15–16% in control-NP-treated cells (Fig. 4D). Our results show that CRISPR/Cas9-PLGA-NPs induced high levels of HbF in HUDEP-2 cells, without affecting cellular viability or phenotype. The expression of HbA was

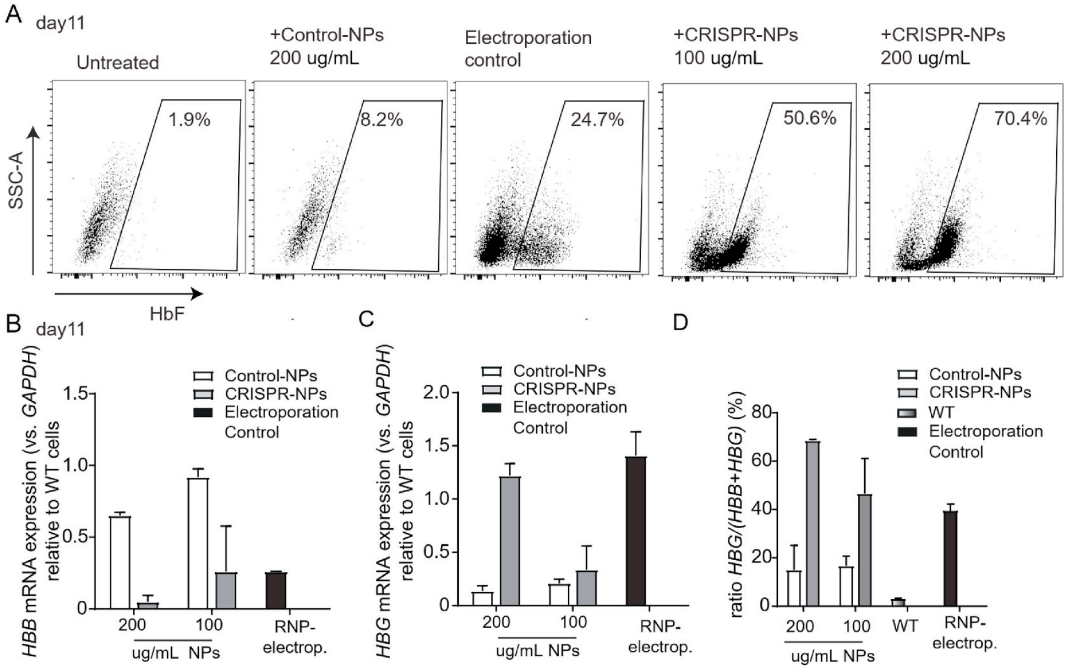

Fig. 4. Upregulation of HbF in HUDEP-2 cells. (A) Representative flow cytometry plots of WT HUDEP-2 cells incubated with 100 μg/mL and 200 μg/mL CRISPR/Cas9-PLGA-NPs, encapsulating a gRNA shown to induce significantly upregulated HbF expression [21], or 200 μg/mL control-NPs encapsulating a scrambled gRNA sequence. As a positive control, sgRNA and Cas9 were electroporated into HUDEP-2 cells using the Neon electroporator. On day 11, the cells were fixed and labelled for intracellular expression of HbF and analysed by flow cytometry. (B) relative *HBB and* (C) *HBG* mRNA expression (vs GAPDH) in HUDEP-2 WT cells, cells treated with control-NPs and CRISPR/Cas9-PLGA-NPs, and electroporated control cells, measured by RT-qPCR on day 11 post NP challenge or electroporation. (D) Percent *HBG* mRNA.

decreased by a similar amount as observed in non-deletion HPFH.

Next, we assessed uptake and gene-editing efficacy of CRISPR/Cas9-PLGA-NPs on primary human erythroblasts, cultured from PBMCs using an erythroid differentiation protocol. In the first phase, erythroid progenitors were expanded until they dominated the cell culture around day 8. Erythroid progenitors were incubated with different concentrations of CRISPR/Cas9-PLGA-NPs (encapsulating the γ-globin promoter targeting sgRNA) and control-NPs, followed by induction of the expansion phase. Three days after NP-incubation (day 11 of erythroblast differentiation), we measured the percentage of NP-positive cells and the intracellular levels of HbF by flow cytometry (Fig. 5A). Similar to the results obtained in HUDEP-2 cells, NPs were readily taken up by erythroblast progenitors in a concentration dependent manner (Fig. 5A). 10% of primary cells expressed HbF and incubation with control-NPs did not increase HbF expression, despite efficient uptake of control-NPs (Fig. 5A). CRISPR/Cas9-PLGA-NPs elevated the levels of HbF in a concentration-dependent manner to 18.1% (50 μg/mL) and 51.7% (200 μg/mL) (Fig. 5A). RT-PCR confirmed a concentration-dependent increase in the percentage of HbF expression at day 3 after treatment with CRISPR/Cas9-PLGA-NPs, but not with control-NPs (Fig. 5B). Analysis of HbF expression over time by flow cytometry showed that the levels of HbF further increased on day 8 and day 14 after treatment with CRISPR/Cas9-PLGA-NPs, while the levels of HbF in WT and control-NP-treated cells remained constant (Fig. 5C). 200 μg/mL and 100 μg/mL CRISPR-Cas9-PLGA-NPs induced high levels of HbF already on day 3, while at 50 μg/mL, increased levels of HbF could be detected on day 8. Genomic analysis of CRISPR/Cas9-PLGA-NPs and control-NP-treated erythroblasts confirmed mutations in the *HBG* promoter region (Fig. 5D). To estimate the frequency and kind of insertions/deletions (indels), we performed TIDE analysis [42] on the Sanger sequencing trace data of the bulk of edited erythroblasts (Fig. 5E). The total indel efficacy was 38.4%, containing insertions as well as deletions. Altogether, our data demonstrates the functionality and efficacy of CRISPR-Cas9-PLGA-NPs in inducing HbF in primary erythroblasts.

3.5. CRISPR/Cas9-PLGA-NP-mediated gene-editing of primary HSPC

The application of CRISPR-Cas9 technology has been hampered by challenges in efficient non-viral expression and delivery of CRISPR components in $CD34^+$ cells, in particular in HSPCs. To evaluate the efficacy of CRISPR/Cas9-PLGA-NPs as delivery system for the CRISPR-RNP complex to HSPCs, we performed uptake studies on isolated human $CD34^+$ cells. Freshly isolated $CD34^+$ cells from PBMCs were incubated with 100 μg/mL CRISPR/Cas9-PLGA-NPs for 1 h at 37 °C and binding and uptake of NPs was evaluated by confocal microscopy (Fig. 6A). CRISPR/Cas9-PLGA-NPs bound and were taken up by different cell types within the population of $CD34^+$ cells, including $CD34^{high}$ cells. We performed additional flow cytometry studies to analyse the binding and uptake behaviour of $CD34^+$ cells. To this end, $CD34^+$ cells were incubated with CRISPR/Cas9-PLGA-NPs at 4 °C, when cells can bind but not take up NPs, and at physiological conditions at 37 °C (Fig. 6B). Binding and uptake of CRISPR/Cas9-PLGA-NPs by $CD34^+$ cells were concentration-dependent. Thus, for further analysis we incubated $CD34^+$ cells with 200 μg/mL CRISPR/Cas9-PLGA-NPs. To evaluate potential cytotoxicity and the gene-editing capacity of CRISPR/Cas9-PLGA-NPs on $CD34^+$ cells, we performed clonal studies on single-cell-derived burst-forming unit-erythroid (BFU-E) colonies grown in methylcellulose culture. To avoid differentiation, $CD34^+$ cells were only shortly incubated with 200 μg/mL CRISPR/Cas9-PLGA-NPs. To increase NP-loading, CRISPR/Cas9-PLGA-NPs were centrifuged on $CD34^+$ cells and NP-loaded cells were directly plated into methylcellulose. Flow cytometry confirmed efficient binding of CRISPR/Cas9-PLGA-NPs to $CD34^+$ cells (Fig. 6C). To assess the number of $Cy5^+$ colonies, the methylcellulose plates were scanned at 700 nm with the Odyssey imaging system (Supplementary Fig. 4).

Almost all colonies derived from $CD34^+$ cells treated with CRISPR/Cas9-PLGA-NPs were $Cy5^+$, while there was no background signal in WT colonies. Further analysis of single clones showed that almost all cells within a colony were $Cy5^+$ (Fig. 6D). There was no difference in the

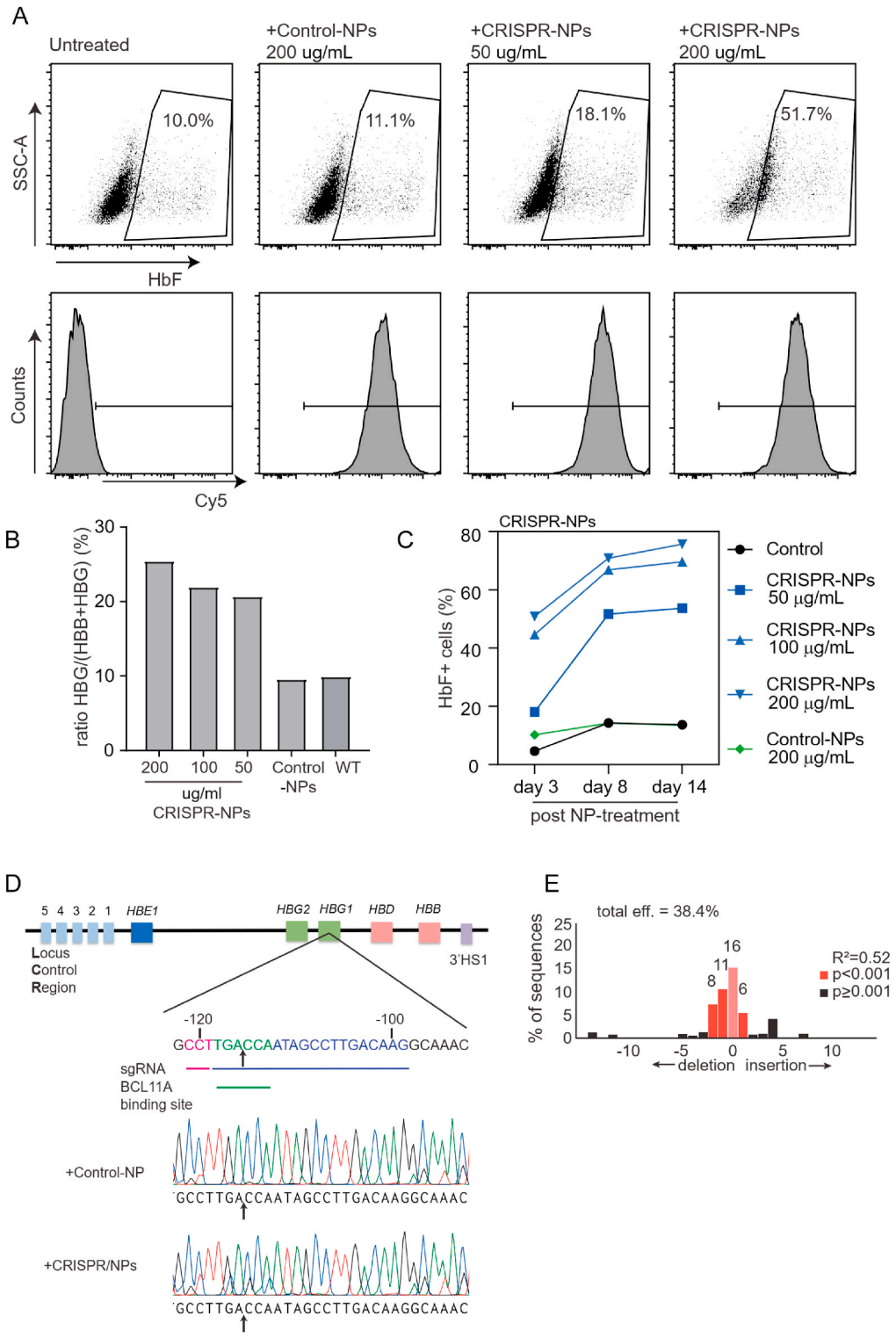

Fig. 5. Upregulation of HbF in primary human erythroblasts. Human PBMCs were differentiated towards erythroblasts and on day 8 (start of phase 2) treated with CRISPR/Cas9-PLGA- or control-NPs. (A) Upper panel, representative flow cytometry plots of HbF expression in primary erythroblasts at day 3 post treatment with 50 μg/mL or 200 μg/mL CRISPR/Cas9-PLGA-NPs, encapsulating sgRNA shown to induce upregulation of HbF [21], or 200 μg/mL control-NPs encapsulating a scrambled sgRNA sequence. Lower panel, % of NP^+ ($Cy5^+$) cells. (B) Percent *HBG* mRNA. (C) % of HbF^+ cells on day 3, 8 and 14 after treatment with 50, 100 or 200 μg/mL CRISPR/Cas9-PLGA-NPs, or 200 μg/mL control-NPs. (D) Top, portrait of the *HBB* locus on chromosome 11. A section of the *HBG1* promoter region indicating spacer (blue) and protospacer adjacent motif (pink), which specify the site of sgRNA-binding and Cas9 cleavage. The gRNA is complementary to the antisense strand. Green nucleotides indicate the BCL11A binding site. The arrow indicates the predicted Cas9-cleavage site. Bottom, Sanger sequencing trace data from primary erythroblasts 14 days after treatment with 200 μg/mL CRISPR/Cas9-PLGA-NPs or control-NPs. (E) TIDE analysis on the sanger sequencing data of the bulk of erythroblasts edited with CRISPR/Cas9-PLGA-NPs. (For interpretation of the references to colour in this figure legend, the reader is referred to the Web version of this article.)

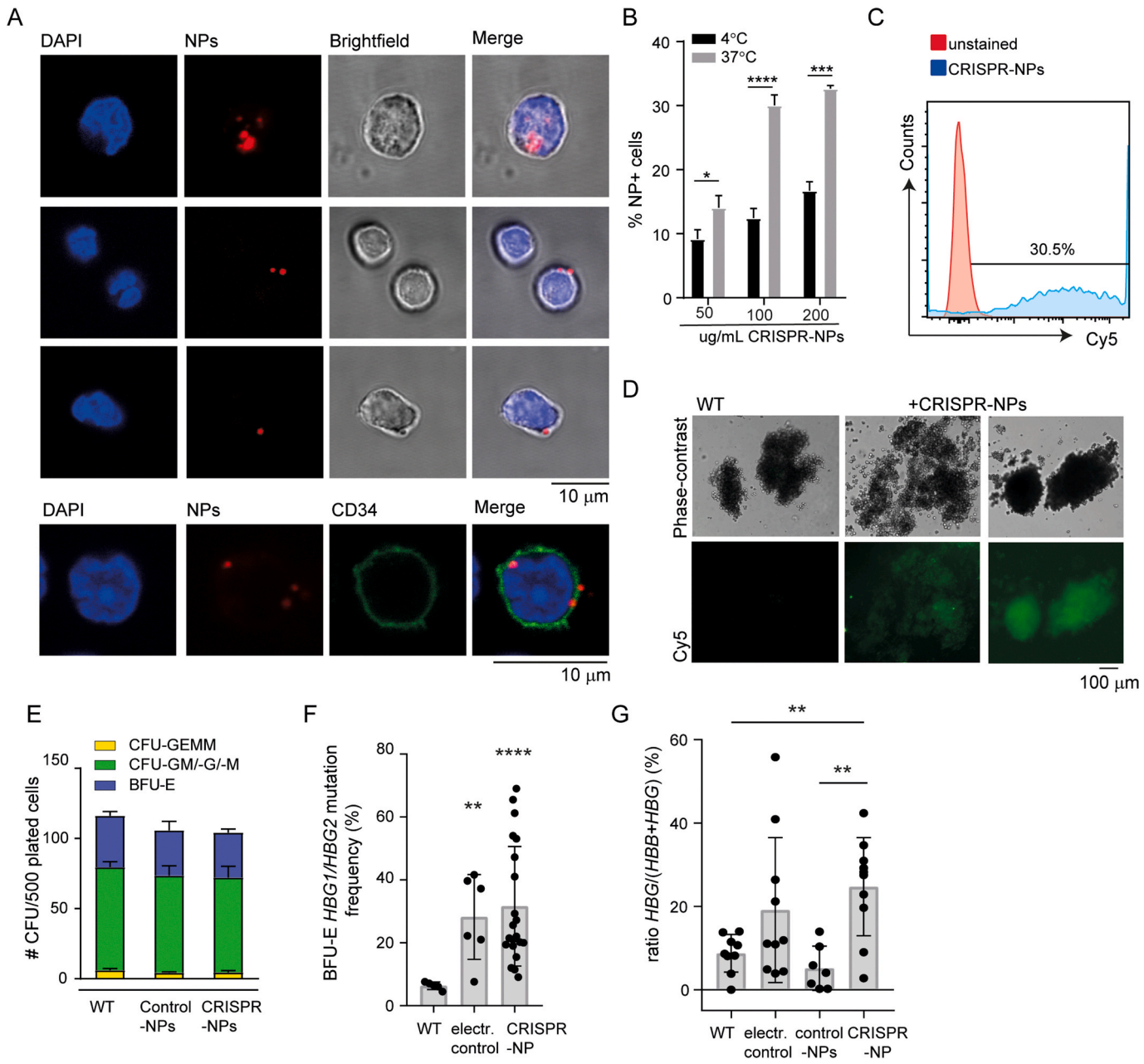

Fig. 6. NP-uptake and gene editing of the *HBG* promoter region in primary human CD34$^+$ cells. (A) Top, representative pictures of isolated CD34$^+$ cells treated with 100 μg/mL CRISPR/Cas9-PLGA-NPs (Cy5, red) for 1 h at 37 °C, analysed by confocal microscopy. Cells were washed and fixed, and stained with DAPI (nucleus = blue). Bottom row, labelling of the cell surface marker CD34 (green) was included. (B) Binding and uptake of CRISPR/Cas9-PLGA-NPs by isolated CD34$^+$ cells after 1 h at 4 °C (binding) or 37 °C (binding and uptake). The data represents the mean ± SEM of 2 independent experiments, including 1 donor. (C) Representative flow cytometry plot of CD34$^+$ cells treated with 200 μg/mL CRISPR/Cas9-PLGA-NPs for 30 min at 37 °C before plating into methylcellulose. (D) Representative images of colonies grown from CD34$^+$ WT cells, or CD34$^+$ cells treated with CRISPR/Cas9-PLGA-NPs, imaged with a fluorescent microscope. NPs (green), scale bar = 100 μm. (E) Hematopoietic progenitor numbers in WT, CRISPR/Cas9-PLGA-NP- or control-NP-treated isolated CD34$^+$ cells. CFU-C (colony forming unit-culture) per 500 sorted cells is shown, with colony types designated by coloured bars: CFU-G = CFU-granulocyte, CFU-M = macrophage and CFU-GM = CFU-granulocyte, macrophage, CFU-GEMM = CFU-granulocyte, erythroid, macrophage, megakaryocyte, and BFU-E = burst forming unit erythroid. (F) TIDE and (G) percent *HBG* mRNA in WT BFU-E colonies, or colonies edited with CRISPR/Cas9-PLGA-NPs or control-NPs. As positive control, the RNP complex was delivered to CD34$^+$ cells by electroporation. Data represent the mean ± SEM of 2 independent experiments. All P-values were compared to the respective control cells using Mann-Whitney test. **=< p 0.0065, ****=< p 0.001. (For interpretation of the references to colour in this figure legend, the reader is referred to the Web version of this article.)

number and type of hematopoietic progenitor colonies derived from WT, CRISPR/Cas9-PLGA-NP and control-NP treated isolated CD34$^+$ cells (Fig. 6E). TIDE analysis of BFU-E colonies from CRISPR/Cas9-PLGA-NPs-treated and electroporated CD34$^+$ cells revealed mutations in the γ-globin promoter region (Fig. 6F). Among the mutations, we identified deletions, as well as insertions. On average 32% and 28% of the screened BFU-E colonies derived from CRISPR/Cas9-PLGA-NP-treated and electroporated CD34$^+$ cells, respectively, had indels and were mosaic for *HBG1/HBG2* mutations (Fig. 6F). This reflects most likely editing over several rounds of cell division. RT-qPCR analysis of individual BFU-E colonies confirmed an increase in HbF mRNA expression in colonies derived from CD34$^+$ cells treated with CRISPR/Cas9-PLGA-NPs and after electroporation (Fig. 6G). Thus, our data indicates that a functional CRISPR-complex was released for a prolonged period of time in CD34$^+$

cells, resulting in highly efficient gene-editing without inducing cellular cytotoxicity.

4. Discussion

CRISPR genome-editing technology has rapidly become a powerful strategy with great potential to cure a large variety of human diseases, including those of the hematopoietic system. However, the delivery of the CRISPR technology to HSPCs remains a challenge. The current state of the art for CRISPR delivery in HSPCs comprises electroporation of the RNP complex and adeno-associated virus (AAV) [44,45] or lentivirus-mediated gene transfer [46–48]. Due to low packaging efficacy, documented immunogenicity of AAV vectors and potential safety issues of the classical vehicles [49,50], non-viral delivery of the RNP complex would be the preferred method. Hematopoietic cells are in general notoriously difficult to transfect using non-viral approaches. Although successful non-viral gene-editing in HSPCs has been reported [14], electroporation of HSPCs remains associated with cellular toxicity [51,52].

In this study, we used PLGA to develop a versatile CRISPR delivery system in erythroid cells and HSPCs. CRISPR/Cas9-PLGA-NPs encapsulated the CRISPR components Cas9 and gRNA (sgRNA or crRNA-tracerRNA hybrid), as well as a fluorescent probe to monitor NP-uptake and intracellular routing. CRISPR/Cas9-PLGA-NPs were extensively characterized and showed efficient loading of Cas9, gRNA and Cy5, while maintaining a uniform size of ~300 nm in diameter and a negative surface charge.

The CRISPR genome-editing components are by nature proteolytically unstable and possess poor membrane permeability potential [29]. Encapsulated inside NPs, Cas9 and gRNA are protected from degradation [23], while the NP core confers new physicochemical properties to the cargo, enabling more efficient uptake of the CRISPR components by the cellular endocytosis machinery. It is well established that NPs smaller than 500 nm enter the cells by pinocytosis [53]. The extent of cellular uptake of PLGA-NPs is influenced by several properties, such as NP size and surface charge, as well as incubation time and NP concentration [54]. In this study, CRISPR/Cas9-PLGA-NPs were successfully taken up by erythroblasts and freshly isolated $CD34^+$ cells in a concentration-dependent manner, despite the lack of a specific targeting moiety. In agreement with previous studies in which PLGA-NPs were applied on $CD34^+$ cells [55], CRISPR/Cas9-PLGA-NPs did not induce cellular cytotoxicity or impaired the hematopoietic potential of $CD34^+$ cells plated in methylcellulose.

Analysis of the intracellular routing in HUDEP-2 cells showed that CRISPR/Cas9-PLGA-NPs were endocytosed in EEA-1 positive vesicles, which matured into lysosomes. In line with previously published data, CRISPR/Cas9-PLGA-NPs escaped the endosomal/lysosomal route and translocated to the cytosol within 24 h after uptake [56]. There are two mechanisms that drive cargo release from PLGA-NPs, initially diffusion and at a later stage degradation of the PLGA core [57]. We showed that the release of Cas9 and gRNA from CRISPR/Cas9-PLGA-NPs followed the typical release profile of standard PLGA NPs: an initial burst release followed by a prolonged period of sustained release [58]. Analysis of the NP physico-chemical properties revealed that CRISPR/Cas9-PLGA-NPs were stable over a period of 7 weeks at 37 °C in PBS. Our microscopy studies further confirmed the dissociation of the Cas9 from the Cy5 signal within 24 h after uptake in HUDEP-2 cells. Both signals appeared more diffuse, compared to the earlier timepoints. Thus, the dominant mechanism of release of Cas9/gRNA from the PLGA-core at early timepoints was likely a result of diffusion.

Using CRISPR/Cas9-PLGA-NPs, we achieved similar editing efficiency in HUDEP-2 cells and primary erythroblasts as reported by *Traxler* et al. using lentiviral transduction [21]. The *HBG* promoter was efficiently targeted in a concentration-dependent manner and high levels of HbF were induced as early as 3 days post NP exposure in erythroblasts. Microscopy data showed that within the pool of isolated $CD34^+$ cells, morphological small and less dense $CD34^{high}$ expressing cells, corresponding to HSPCs [59], bound and took up CRISPR/Cas9-PLGA-NPs 1 h after NP exposure, albeit at lower rates than larger and denser $CD34^{low}$ cells, presenting colony forming units-granulocyte macrophage (CFU-GM) [59]. Flow cytometry data further showed that the uptake of CRISPR/Cas9-PLGA-NPs by HSPCs was dependent on NP concentration. Despite the initial difference in NP-uptake among $CD34^+$ cells, CRISPR/Cas9-PLGA-NPs were efficiently taken up by erythroid progenitors, as on average 40% of analysed BFU-E colonies showed indels in the targeted *HBG1/HBG2* promoter loci. All analysed colonies were mosaic for *HBG1/HBG2* mutations, indicating that after the initial burst release, the CRISPR components were released slowly and remained functional during proliferation of methylcellulose colonies. In summary, this establishes CRISPR/Cas9-PLGA-NPs as an efficient non-viral delivery system for CRISPR/Cas9 to HSPCs.

β-hemoglobinopathies are most prevalent in developing countries. A reliable, efficient, easy-to-use and cost-effective delivery method could provide treatment to more patients. CRISPR/Cas9-PLGA-NPs address several limitations to the current state of the art for HSPC gene editing, such as electroporation-associated toxicity and efficacy of RNP complex delivery inside target cells *ex vivo* and *in vivo*. The latter is a prerequisite to take CRISPR/Cas9 forward to broader clinical applications. Encapsulation of CRISPR/Cas9 inside NPs and targeted delivery improves the ratio efficacy/toxicity, and less Cas9 is needed to perform gene-editing as the CRISPR-complex is targeted to and taken up by the right cell type/tissue. This could help towards overcoming manufacturing challenges of GMP-quality Cas9 for clinical application, as encapsulated drugs in PLGA allows an about 10-1000-fold increase in the efficiency of drug compounds [60]. Importantly, CRISPR/Cas9-PLGA-NPs are versatile and could be adapted to other gene-editing tools, such as adenine and cytosine base editors [61].

To successfully translate CRISPR/Cas9-PLGA-NPs to clinical application, some limitations in the efficacy of PLGA delivery systems need to be addressed, such as the initial rapid (burst) release of the payload, that we also observed in this study [62,63]. This could affect the concentration of CRISPR/Cas9 in target cells *in vivo*. Changes in PLGA composition (e.g. molecular weight or the composition ratio of lactide: glycolide), incorporation of a second protecting layer (e.g. PEGylation) on the PLGA-NP surface to avoid premature diffusion, or novel 'smart" polymers featuring a spatiotemporal controlled release kinetics [64] could address these limitations and improve the efficacy of CRISPR/Cas9-PLGA-NPs. Another limitation for clinical translation is the rapid clearance of circulating NPs after systemic administration. Surface modification by PEGylation [31,34,65] and targeting ligand functionalization [32] are important factors to improve the blood circulation half-life by reducing the level of nonspecific uptake and to increase specificity towards target cells *in vivo*, respectively. For efficient uptake by HSCs *in vivo*, CRISPR/Cas9-PLGA-NPs would need to reach the bone marrow, which represents the major HSPC niche in adults. Several strategies using bone-targeting peptides, small molecule ligands and membrane coatings conjugated to the NP surface have been employed to increase the localization of NPs to the bone marrow [66,67]. These strategies could potentially be combined with CRISPR/Cas9-PLGA-NPs to confer specificity towards HSPCs for future applications *in vivo*.

In summary, this study demonstrates the feasibility of utilizing the advantageous properties of PLGA for efficient and safe delivery of the CRISPR gene-editing machinery in HSPCs and provides a basis to bridge the gap between bench and bedside by taking CRISPR/Cas9 forward to broader clinical applications.

Data availability

The authors declare that all data supporting this study are available within the manuscript or can be obtained from the authors upon request.

Author contributions

LJC, TvD, OV, TMWYL, FB, TS and CE performed the experiments. RK and YN provided HUDEP-2 WT cells for this study. CE, LJC, FG and SP designed the experiments and CE and LJC coordinated the study. LJC and CE wrote the manuscript and TvD, FG and SP provided input to the manuscript.

Declaration of competing interest

The authors declare that they have no known competing financial interests or personal relationships that could have appeared to influence the work reported in this paper.

Acknowledgements

L.J.C. was supported by project grants from the European Commission H2020-MSCA-RISE (644373 - PRISAR), H2020-MSCA-RISE (777682 - CANCER), H2020-WIDESPREAD-05-2017-Twinning (807281 - ACORN), H2020-WIDESPREAD-2018-03 (852985 - SIMICA), H2020-SCA-RISE-2016 (734684 - CHARMED) and MSCA-ITN-2015-ETN (675743-ISPIC), 861190 (PAVE), 857894 (CAST), 859908 (NOVA-MRI); 872860 (PRISAR2). L.J.C was also supported by the research program VIDI (project number 723.012.110) of Dutch Research Council (NWO). S.P., F.G. and T.B.vD. were supported by the Landsteiner Foundation for Blood Transfusion Research (LSBR 1627), the Netherlands Organization for Scientific Research (ZonMw TOP 40-00812-98-12128), and EU fp7 Specific Cooperation Research Project THALAMOSS (306201). C.E. was supported by the research program VENI with project number 916.181.54, which is (partly) financed by the Dutch Research Council (NWO) and by the H2020-WIDESPREAD-2018-03 (852985 - SIMICA) project grant from the European Commission. In addition, this study was co-funded by the Dutch PPS allowance made available by Health~-Holland, Top Sector Life Sciences & Health for the project NANOCAST (1 and 2).

Appendix A. Supplementary data

Supplementary data to this article can be found online at https://doi.org/10.1016/j.biomaterials.2020.120580.

References

[1] M.J. Stuart, R.L. Nagel, Sickle-cell disease, Lancet 364 (9442) (2004) 1343–1360.
[2] M.H. Steinberg, Sickle cell anemia, the first molecular disease: overview of molecular etiology, pathophysiology, and therapeutic approaches, ScientificWorldJournal 8 (2008) 1295–1324.
[3] K.J. Wierenga, I.R. Hambleton, N.A. Lewis, Survival estimates for patients with homozygous sickle-cell disease in Jamaica: a clinic-based population study, Lancet 357 (9257) (2001) 680–683.
[4] G. Lucarelli, A. Isgro, P. Sodani, J. Gaziev, Hematopoietic stem cell transplantation in thalassemia and sickle cell anemia, Cold Spring Harb Perspect Med 2 (5) (2012) a011825.
[5] J.V. Raja, M.A. Rachchh, R.H. Gokani, Recent advances in gene therapy for thalassemia, J. Pharm. BioAllied Sci. 4 (3) (2012) 194–201.
[6] D.S. Vinjamur, D.E. Bauer, S.H. Orkin, Recent progress in understanding and manipulating haemoglobin switching for the haemoglobinopathies, Br. J. Haematol. 180 (5) (2018) 630–643.
[7] D.E. Bauer, S.C. Kamran, S.H. Orkin, Reawakening fetal hemoglobin: prospects for new therapies for the beta-globin disorders, Blood 120 (15) (2012) 2945–2953.
[8] C. Brendel, S. Guda, R. Renella, D.E. Bauer, M.C. Canver, Y.J. Kim, M.M. Heeney, D. Klatt, J. Fogel, M.D. Milsom, S.H. Orkin, R.I. Gregory, D.A. Williams, Lineage-specific BCL11A knockdown circumvents toxicities and reverses sickle phenotype, J. Clin. Invest. 126 (10) (2016) 3868–3878.
[9] M.C. Canver, E.C. Smith, F. Sher, L. Pinello, N.E. Sanjana, O. Shalem, D.D. Chen, P. G. Schupp, D.S. Vinjamur, S.P. Garcia, S. Luc, R. Kurita, Y. Nakamura, Y. Fujiwara, T. Maeda, G.C. Yuan, F. Zhang, S.H. Orkin, D.E. Bauer, BCL11A enhancer dissection by Cas9-mediated in situ saturating mutagenesis, Nature 527 (7577) (2015) 192–197.
[10] K.H. Chang, S.E. Smith, T. Sullivan, K. Chen, Q. Zhou, J.A. West, M. Liu, Y. Liu, B. F. Vieira, C. Sun, V.P. Hong, M. Zhang, X. Yang, A. Reik, F.D. Urnov, E.J. Rebar, M. C. Holmes, O. Danos, H. Jiang, S. Tan, Long-term engraftment and fetal globin induction upon BCL11A gene editing in bone-marrow-derived CD34(+) hematopoietic stem and progenitor cells, Mol Ther Methods Clin Dev 4 (2017) 137–148.
[11] F.C. Costa, H. Fedosyuk, R. Neades, J.B. de Los Rios, C.F. Barbas 3rd, K.R. Peterson, Induction of fetal hemoglobin in vivo mediated by a synthetic gamma-globin zinc finger activator, Anemia 2012 (2012) 507894.
[12] D.P. Dever, R.O. Bak, A. Reinisch, J. Camarena, G. Washington, C.E. Nicolas, M. Pavel-Dinu, N. Saxena, A.B. Wilkens, S. Mantri, N. Uchida, A. Hendel, A. Narla, R. Majeti, K.I. Weinberg, M.H. Porteus, CRISPR/Cas9 beta-globin gene targeting in human haematopoietic stem cells, Nature 539 (7629) (2016) 384–389.
[13] M.A. DeWitt, W. Magis, N.L. Bray, T. Wang, J.R. Berman, F. Urbinati, S.J. Heo, T. Mitros, D.P. Munoz, D. Boffelli, D.B. Kohn, M.C. Walters, D. Carroll, D.I. Martin, J.E. Corn, Selection-free genome editing of the sickle mutation in human adult hematopoietic stem/progenitor cells, Sci. Transl. Med. 8 (360) (2016), 360ra134.
[14] O. Humbert, S. Radtke, C. Samuelson, R.R. Carrillo, A.M. Perez, S.S. Reddy, C. Lux, S. Pattabhi, L.E. Schefter, O. Negre, C.M. Lee, G. Bao, J.E. Adair, C.W. Peterson, D. J. Rawlings, A.M. Scharenberg, H.P. Kiem, Therapeutically relevant engraftment of a CRISPR-Cas9-edited HSC-enriched population with HbF reactivation in nonhuman primates, Sci. Transl. Med. 11 (503) (2019).
[15] S.H. Park, C.M. Lee, D.P. Dever, T.H. Davis, J. Camarena, W. Srifa, Y. Zhang, A. Paikari, A.K. Chang, M.H. Porteus, V.A. Sheehan, G. Bao, Highly efficient editing of the beta-globin gene in patient-derived hematopoietic stem and progenitor cells to treat sickle cell disease, Nucleic Acids Res. 47 (15) (2019) 7955–7972.
[16] A. Perumbeti, T. Higashimoto, F. Urbinati, R. Franco, H.J. Meiselman, D. Witte, P. Malik, A novel human gamma-globin gene vector for genetic correction of sickle cell anemia in a humanized sickle mouse model: critical determinants for successful correction, Blood 114 (6) (2009) 1174–1185.
[17] J.A. Ribeil, S. Hacein-Bey-Abina, E. Payen, A. Magnani, M. Semeraro, E. Magrin, L. Caccavelli, B. Neven, P. Bourget, W. El Nemer, P. Bartolucci, L. Weber, H. Puy, J. F. Meritet, D. Grevent, Y. Beuzard, S. Chretien, T. Lefebvre, R.W. Ross, O. Negre, G. Veres, L. Sandler, S. Soni, M. de Montalembert, S. Blanche, P. Leboulch, M. Cavazzana, Gene therapy in a patient with sickle cell disease, N. Engl. J. Med. 376 (9) (2017) 848–855.
[18] B. Wienert, A.P. Funnell, L.J. Norton, R.C. Pearson, L.E. Wilkinson-White, K. Lester, J. Vadolas, M.H. Porteus, J.M. Matthews, K.G. Quinlan, M. Crossley, Editing the genome to introduce a beneficial naturally occurring mutation associated with increased fetal globin, Nat. Commun. 6 (2015) 7085.
[19] J. Yen, M. Fiorino, Y. Liu, S. Paula, S. Clarkson, L. Quinn, W.R. Tschantz, H. Klock, N. Guo, C. Russ, V.W.C. Yu, C. Mickanin, S.C. Stevenson, C. Lee, Y. Yang, TRIAMF: a new method for delivery of Cas9 ribonucleoprotein complex to human hematopoietic stem cells, Sci. Rep. 8 (1) (2018) 16304.
[20] J.Y. Metais, P.A. Doerfler, T. Mayuranathan, D.E. Bauer, S.C. Fowler, M.M. Hsieh, V. Katta, S. Keriwala, C.R. Lazzarotto, K. Luk, M.D. Neel, S.S. Perry, S.T. Peters, S. N. Porter, B.Y. Ryu, A. Sharma, D. Shea, J.F. Tisdale, N. Uchida, S.A. Wolfe, K. J. Woodard, Y. Wu, Y. Yao, J. Zeng, S. Pruett-Miller, S.Q. Tsai, M.J. Weiss, Genome editing of HBG1 and HBG2 to induce fetal hemoglobin, Blood Adv 3 (21) (2019) 3379–3392.
[21] E.A. Traxler, Y. Yao, Y.D. Wang, K.J. Woodard, R. Kurita, Y. Nakamura, J. R. Hughes, R.C. Hardison, G.A. Blobel, C. Li, M.J. Weiss, A genome-editing strategy to treat beta-hemoglobinopathies that recapitulates a mutation associated with a benign genetic condition, Nat. Med. 22 (9) (2016) 987–990.
[22] M.C. Gundry, L. Brunetti, A. Lin, A.E. Mayle, A. Kitano, D. Wagner, J.I. Hsu, K. A. Hoegenauer, C.M. Rooney, M.A. Goodell, D. Nakada, Highly efficient genome editing of murine and human hematopoietic progenitor cells by CRISPR/Cas9, Cell Rep. 17 (5) (2016) 1453–1461.
[23] M. Wang, J.A. Zuris, F. Meng, H. Rees, S. Sun, P. Deng, Y. Han, X. Gao, D. Pouli, Q. Wu, I. Georgakoudi, D.R. Liu, Q. Xu, Efficient delivery of genome-editing proteins using bioreducible lipid nanoparticles, Proc. Natl. Acad. Sci. U. S. A. 113 (11) (2016) 2868–2873.
[24] D.S. D'Astolfo, R.J. Pagliero, A. Pras, W.R. Karthaus, H. Clevers, V. Prasad, R. J. Lebbink, H. Rehmann, N. Geijsen, Efficient intracellular delivery of native proteins, Cell 161 (3) (2015) 674–690.
[25] J.S. Ha, J.S. Lee, J. Jeong, H. Kim, J. Byun, S.A. Kim, H.J. Lee, H.S. Chung, J.B. Lee, D.R. Ahn, Poly-sgRNA/siRNA ribonucleoprotein nanoparticles for targeted gene disruption, J. Contr. Release 250 (2017) 27–35.
[26] J.B. Miller, S. Zhang, P. Kos, H. Xiong, K. Zhou, S.S. Perelman, H. Zhu, D. J. Siegwart, Non-viral CRISPR/Cas gene editing in vitro and in vivo enabled by synthetic nanoparticle Co-delivery of Cas9 mRNA and sgRNA, Angew Chem. Int. Ed. Engl. 56 (4) (2017) 1059–1063.
[27] S. Ramakrishna, A.B. Kwaku Dad, J. Beloor, R. Gopalappa, S.K. Lee, H. Kim, Gene disruption by cell-penetrating peptide-mediated delivery of Cas9 protein and guide RNA, Genome Res. 24 (6) (2014) 1020–1027.
[28] A. Hendel, R.O. Bak, J.T. Clark, A.B. Kennedy, D.E. Ryan, S. Roy, I. Steinfeld, B. D. Lunstad, R.J. Kaiser, A.B. Wilkens, R. Bacchetta, A. Tsalenko, D. Dellinger, L. Bruhn, M.H. Porteus, Chemically modified guide RNAs enhance CRISPR-Cas genome editing in human primary cells, Nat. Biotechnol. 33 (9) (2015) 985–989.
[29] A. Fu, R. Tang, J. Hardie, M.E. Farkas, V.M. Rotello, Promises and pitfalls of intracellular delivery of proteins, Bioconjugate Chem. 25 (9) (2014) 1602–1608.
[30] F. Danhier, E. Ansorena, J.M. Silva, R. Coco, A. Le Breton, V. Preat, PLGA-based nanoparticles: an overview of biomedical applications, J. Contr. Release 161 (2) (2012) 505–522.
[31] L.J. Cruz, P.J. Tacken, R. Fokkink, C.G. Figdor, The influence of PEG chain length and targeting moiety on antibody-mediated delivery of nanoparticle vaccines to human dendritic cells, Biomaterials 32 (28) (2011) 6791–6803.
[32] L.J. Cruz, P.J. Tacken, J.M. Pots, R. Torensma, S.I. Buschow, C.G. Figdor, Comparison of antibodies and carbohydrates to target vaccines to human dendritic cells via DC-SIGN, Biomaterials 33 (16) (2012) 4229–4239.

[33] R.A. Rosalia, L.J. Cruz, S. van Duikeren, A.T. Tromp, A.L. Silva, W. Jiskoot, T. de Gruijl, C. Lowik, J. Oostendorp, S.H. van der Burg, F. Ossendorp, CD40-targeted dendritic cell delivery of PLGA-nanoparticle vaccines induce potent anti-tumor responses, Biomaterials 40 (2015) 88–97.
[34] L.J. Cruz, P.J. Tacken, R. Fokkink, B. Joosten, M.C. Stuart, F. Albericio, R. Torensma, C.G. Figdor, Targeted PLGA nano- but not microparticles specifically deliver antigen to human dendritic cells via DC-SIGN in vitro, J. Contr. Release 144 (2) (2010) 118–126.
[35] C. Perez, A. Sanchez, D. Putnam, D. Ting, R. Langer, M.J. Alonso, Poly(lactic acid)-poly(ethylene glycol) nanoparticles as new carriers for the delivery of plasmid DNA, J. Contr. Release 75 (1–2) (2001) 211–224.
[36] D. Luo, K. Woodrow-Mumford, N. Belcheva, W.M. Saltzman, Controlled DNA delivery systems, Pharm. Res. (N. Y.) 16 (8) (1999) 1300–1308.
[37] G. Dordelmann, D. Kozlova, S. Karczewski, R. Lizio, S. Knauer, M. Epple, Calcium phosphate increases the encapsulation efficiency of hydrophilic drugs (proteins, nucleic acids) into poly(d,l-lactide-co-glycolide acid) nanoparticles for intracellular delivery, J. Mater. Chem. B 2 (41) (2014) 7250–7259.
[38] R. Kurita, N. Suda, K. Sudo, K. Miharada, T. Hiroyama, H. Miyoshi, K. Tani, Y. Nakamura, Establishment of immortalized human erythroid progenitor cell lines able to produce enucleated red blood cells, PloS One 8 (3) (2013), e59890.
[39] L. Ronzoni, P. Bonara, D. Rusconi, C. Frugoni, I. Libani, M.D. Cappellini, Erythroid differentiation and maturation from peripheral CD34+ cells in liquid culture: cellular and molecular characterization, Blood Cells Mol. Dis. 40 (2) (2008) 148–155.
[40] E. van den Akker, T.J. Satchwell, S. Pellegrin, G. Daniels, A.M. Toye, The majority of the in vitro erythroid expansion potential resides in CD34(-) cells, outweighing the contribution of CD34(+) cells and significantly increasing the erythroblast yield from peripheral blood samples, Haematologica 95 (9) (2010) 1594–1598.
[41] A. Medvinsky, S. Taoudi, S. Mendes, E. Dzierzak, Analysis and manipulation of hematopoietic progenitor and stem cells from murine embryonic tissues, Curr Protoc Stem Cell Biol Chapter 2 (2008). Unit 2A 6.
[42] E.K. Brinkman, T. Chen, M. Amendola, B. van Steensel, Easy quantitative assessment of genome editing by sequence trace decomposition, Nucleic Acids Res. 42 (22) (2014) e168.
[43] D. Cun, D.K. Jensen, M.J. Maltesen, M. Bunker, P. Whiteside, D. Scurr, C. Foged, H. M. Nielsen, High loading efficiency and sustained release of siRNA encapsulated in PLGA nanoparticles: quality by design optimization and characterization, Eur. J. Pharm. Biopharm. 77 (1) (2011) 26–35.
[44] B.D. Sather, G.S. Romano Ibarra, K. Sommer, G. Curinga, M. Hale, I.F. Khan, S. Singh, Y. Song, K. Gwiazda, J. Sahni, J. Jarjour, A. Astrakhan, T.A. Wagner, A. M. Scharenberg, D.J. Rawlings, Efficient modification of CCR5 in primary human hematopoietic cells using a megaTAL nuclease and AAV donor template, Sci. Transl. Med. 7 (307) (2015), 307ra156.
[45] L. Song, X. Li, G.R. Jayandharan, Y. Wang, G.V. Aslanidi, C. Ling, L. Zhong, G. Gao, M.C. Yoder, C. Ling, M. Tan, A. Srivastava, High-efficiency transduction of primary human hematopoietic stem cells and erythroid lineage-restricted expression by optimized AAV6 serotype vectors in vitro and in a murine xenograft model in vivo, PloS One 8 (3) (2013), e58757.
[46] A. Aiuti, L. Biasco, S. Scaramuzza, F. Ferrua, M.P. Cicalese, C. Baricordi, F. Dionisio, A. Calabria, S. Giannelli, M.C. Castiello, M. Bosticardo, C. Evangelio, A. Assanelli, M. Casiraghi, S. Di Nunzio, L. Callegaro, C. Benati, P. Rizzardi, D. Pellin, C. Di Serio, M. Schmidt, C. Von Kalle, J. Gardner, N. Mehta, V. Neduva, D.J. Dow, A. Galy, R. Miniero, A. Finocchi, A. Metin, P.P. Banerjee, J.S. Orange, S. Galimberti, M.G. Valsecchi, A. Biffi, E. Montini, A. Villa, F. Ciceri, M. G. Roncarolo, L. Naldini, Lentiviral hematopoietic stem cell gene therapy in patients with Wiskott-Aldrich syndrome, Science 341 (6148) (2013) 1233151.
[47] J. Kanter, M.C. Walters, M. Hsieh, L. Krishnamurti, J.L. Kwiatkowski, R. Kamble, C. von Kalle, M. Joseney-Antoine, F.J. Pierciey Jr., W. Shi, M. Asmal, A. A. Thompson, J.F. Tisdale, Interim results from a phase 1/2 clinical study of lentiglobin gene therapy for severe sickle cell disease, Blood 130 (Supplement 1) (2017), 527-527.
[48] A.A. Thompson, M.C. Walters, J. Kwiatkowski, J.E.J. Rasko, J.A. Ribeil, S. Hongeng, E. Magrin, G.J. Schiller, E. Payen, M. Semeraro, D. Moshous, F. Lefrere, H. Puy, P. Bourget, A. Magnani, L. Caccavelli, J.S. Diana, F. Suarez, F. Monpoux, V. Brousse, C. Poirot, C. Brouzes, J.F. Meritet, C. Pondarre, Y. Beuzard, S. Chretien, T. Lefebvre, D.T. Teachey, U. Anurathapan, P.J. Ho, C. von Kalle, M. Kletzel, E. Vichinsky, S. Soni, G. Veres, O. Negre, R.W. Ross, D. Davidson, A. Petrusich, L. Sandler, M. Asmal, O. Hermine, M. De Montalembert, S. Hacein-Bey-Abina, S. Blanche, P. Leboulch, M. Cavazzana, Gene therapy in patients with transfusion-dependent beta-thalassemia, N. Engl. J. Med. 378 (16) (2018) 1479–1493.
[49] Z. Wu, H. Yang, P. Colosi, Effect of genome size on AAV vector packaging, Mol. Ther. 18 (1) (2010) 80–86.
[50] H. Yin, R.L. Kanasty, A.A. Eltoukhy, A.J. Vegas, J.R. Dorkin, D.G. Anderson, Non-viral vectors for gene-based therapy, Nat. Rev. Genet. 15 (8) (2014) 541–555.
[51] P.K. Mandal, L.M. Ferreira, R. Collins, T.B. Meissner, C.L. Boutwell, M. Friesen, V. Vrbanac, B.S. Garrison, A. Stortchevoi, D. Bryder, K. Musunuru, H. Brand, A. M. Tager, T.M. Allen, M.E. Talkowski, D.J. Rossi, C.A. Cowan, Efficient ablation of genes in human hematopoietic stem and effector cells using CRISPR/Cas9, Cell Stem Cell 15 (5) (2014) 643–652.
[52] S.R. Modarai, D. Man, P. Bialk, N. Rivera-Torres, K. Bloh, E.B. Kmiec, Efficient delivery and nuclear uptake is not sufficient to detect gene editing in CD34+ cells directed by a ribonucleoprotein complex, Mol. Ther. Nucleic Acids 11 (2018) 116–129.
[53] J. Zhao, M.H. Stenzel, Entry of nanoparticles into cells: the importance of nanoparticle properties, Polym. Chem. 9 (3) (2018) 259–272.
[54] S. Xiong, X. Zhao, B.C. Heng, K.W. Ng, J.S. Loo, Cellular uptake of Poly-(D,L-lactide-co-glycolide) (PLGA) nanoparticles synthesized through solvent emulsion evaporation and nanoprecipitation method, Biotechnol. J. 6 (5) (2011) 501–508.
[55] N.A. McNeer, J.Y. Chin, E.B. Schleifman, R.J. Fields, P.M. Glazer, W.M. Saltzman, Nanoparticles deliver triplex-forming PNAs for site-specific genomic recombination in CD34+ human hematopoietic progenitors, Mol. Ther. 19 (1) (2011) 172–180.
[56] L.J. Cruz, P.J. Tacken, I.S. Zeelenberg, M. Srinivas, F. Bonetto, B. Weigelin, C. Eich, I.J. de Vries, C.G. Figdor, Tracking targeted bimodal nanovaccines: immune responses and routing in cells, tissue, and whole organism, Mol. Pharm. 11 (12) (2014) 4299–4313.
[57] N. Kamaly, B. Yameen, J. Wu, O.C. Farokhzad, Degradable controlled-release polymers and polymeric nanoparticles: mechanisms of controlling drug release, Chem. Rev. 116 (4) (2016) 2602–2663.
[58] L. Zerrillo, I. Que, O. Vepris, L.N. Morgado, A. Chan, K. Bierau, Y. Li, F. Galli, E. Bos, R. Censi, P. Di Martino, G. van Osch, L.J. Cruz, pH-responsive poly(lactide-co-glycolide) nanoparticles containing near-infrared dye for visualization and hyaluronic acid for treatment of osteoarthritis, J. Contr. Release 309 (2019) 265–276.
[59] G. Herbein, H. Sovalat, E. Wunder, M. Baerenzung, J. Bachorz, H. Lewandowski, C. Schweitzer, C. Schmitt, A. Kirn, P. Henon, Isolation and identification of two CD34+ cell subpopulations from normal human peripheral blood, Stem Cell. 12 (2) (1994) 187–197.
[60] A.L. Silva, P.C. Soema, B. Slutter, F. Ossendorp, W. Jiskoot, PLGA particulate delivery systems for subunit vaccines: linking particle properties to immunogenicity, Hum. Vaccines Immunother. 12 (4) (2016) 1056–1069.
[61] Y. Yu, T.C. Leete, D.A. Born, L. Young, L.A. Barrera, S.-J. Lee, H.A. Rees, G. Ciaramella, N.M. Gaudelli, Cytosine base editors with minimized unguided DNA and RNA off-target events and high on-target activity, Nat. Commun. 11 (1) (2020) 2052.
[62] D. Blanco, M.J. Alonso, Protein encapsulation and release from poly(lactide-co-glycolide) microspheres: effect of the protein and polymer properties and of the co-encapsulation of surfactants, Eur. J. Pharm. Biopharm. 45 (3) (1998) 285–294.
[63] T. Estey, J. Kang, S.P. Schwendeman, J.F. Carpenter, BSA degradation under acidic conditions: a model for protein instability during release from PLGA delivery systems, J. Pharmaceut. Sci. 95 (7) (2006) 1626–1639.
[64] S. Rezaei, S. Kashanian, Y. Bahrami, L.J. Cruz, M. Motiei, Redox-sensitive and hyaluronic acid-functionalized nanoparticles for improving breast cancer treatment by cytoplasmic 17α-methyltestosterone delivery, Molecules 25 (5) (2020).
[65] J.S. Suk, Q. Xu, N. Kim, J. Hanes, L.M. Ensign, PEGylation as a strategy for improving nanoparticle-based drug and gene delivery, Adv. Drug Deliv. Rev. 99 (Pt A) (2016) 28–51.
[66] V. Chander, G. Gangenahalli, Pluronic-F127/Platelet Microvesicles nanocomplex delivers stem cells in high doses to the bone marrow and confers post-irradiation survival, Sci. Rep. 10 (1) (2020) 156.
[67] A. Swami, M.R. Reagan, P. Basto, Y. Mishima, N. Kamaly, S. Glavey, S. Zhang, M. Moschetta, D. Seevaratnam, Y. Zhang, J. Liu, M. Memarzadeh, J. Wu, S. Manier, J. Shi, N. Bertrand, Z.N. Lu, K. Nagano, R. Baron, A. Sacco, A.M. Roccaro, O. C. Farokhzad, I.M. Ghobrial, Engineered nanomedicine for myeloma and bone microenvironment targeting, Proc. Natl. Acad. Sci. Unit. States Am. 111 (28) (2014) 10287–10292.